NASA TECHNICAL NOTE

NASA TN D-3374

NASA TN D-3374

HYPERSONIC AERODYNAMIC CHARACTERISTICS OF AIRCRAFT CONFIGURATIONS WITH CANARD CONTROLS

by Cuyler W. Brooks, Jr., and Clarence D. Cone, Jr.

Langley Research Center
Langley Station, Hampton, Va.

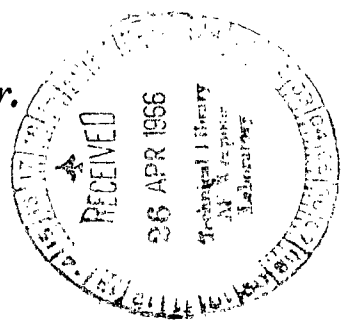

NATIONAL AERONAUTICS AND SPACE ADMINISTRATION • WASHINGTON, D. C. • APRIL 1966

NASA TN D-3374

HYPERSONIC AERODYNAMIC CHARACTERISTICS OF AIRCRAFT CONFIGURATIONS WITH CANARD CONTROLS

By Cuyler W. Brooks, Jr., and Clarence D. Cone, Jr.

Langley Research Center
Langley Station, Hampton, Va.

NATIONAL AERONAUTICS AND SPACE ADMINISTRATION

For sale by the Clearinghouse for Federal Scientific and Technical Information
Springfield, Virginia 22151 – Price $0.85

HYPERSONIC AERODYNAMIC CHARACTERISTICS OF AIRCRAFT CONFIGURATIONS WITH CANARD CONTROLS

By Cuyler W. Brooks, Jr., and Clarence D. Cone, Jr.
Langley Research Center

SUMMARY

An experimental investigation of the aerodynamic characteristics of a canard-control, wing-body configuration having a 70°-swept-delta wing was made at a Mach number of 10.03 in the Langley hypersonic flow apparatus. The effects of canard size and planform, body length, wing position, and vertical-tail position on the longitudinal, lateral, and directional characteristics were determined.

The results indicate that the stability and lift characteristics of these configurations are nonlinear because of the nature of the hypersonic flow regime; these experimental nonlinearities are qualitatively predicted by Newtonian impact theory. However, the effects of canard deflection and wing vertical position on the variation of lift coefficient with angle of attack indicate that there is a measurable interference effect of the canard shock field and/or wake on the flow under the high wing.

Canard control effectiveness is somewhat greater for the trapezoidal than for the delta canard. Canard control effectiveness also increases with body length (canard moment arm) for the high-wing configurations, whereas for the low-wing configurations an increase is found only for the highest canard deflection.

The canards have negligible effects on the lateral and directional stability of the configurations except at the higher angles of attack. The vertical tails are directionally stabilizing, as would be expected, but the dihedral effect of the vertical tails is dependent on the wing vertical position. The high-wing configurations are considerably more stable laterally and directionally than the corresponding low-wing configurations.

INTRODUCTION

There has been considerable interest in the past in the use of canard controls at supersonic Mach numbers because of the greater control effectiveness and high maximum lift-drag ratios obtainable with these controls compared with those obtainable with conventional aft-tail controls. (See refs. 1 to 4.) In experimental investigations of various hypersonic configurations, it has been found that conventional rearward pitch controls

lose effectiveness when they come within the hypersonic "shadow region." (See ref. 5.) Since canard controls are not subject to this blanketing effect, because of their forward location, and since canards have been found to be effective control devices at supersonic speeds, the question of their value at the higher Mach numbers for use in various hypersonic cruise-vehicle concepts is of interest.

The purpose of the present investigation was to determine the characteristics of a generalized aircraft configuration utilizing canard control surfaces at hypersonic speeds. The effects of such variables as canard size, planform, moment arm, wing position, and vertical tails were included in the investigation. The investigation was made in the Langley 15-inch hypersonic flow apparatus at a Mach number of 10.03. The Reynolds number was 1.5×10^6 per foot $\left(4.92 \times 10^6 \text{ per meter}\right)$. Canard deflections of 0°, 5°, 10°, and 20° were tested. The angle-of-attack range was -4° to 20° at 0° sideslip angle; a few selected configurations were tested through the same angle-of-attack range at -5° sideslip. Some of these configurations were also tested through a sideslip-angle range of -9° to 3° at an angle of attack of zero.

SYMBOLS

The longitudinal force and moment coefficients are referred to the stability system of axes with the origin on the fuselage center line at 60 percent of the total body length. The lateral coefficients are referred to the body system of axes.

a	canard moment arm about moment reference center
b	wing span
c	local chord length (wing or canard)
$\bar{c}$	mean aerodynamic chord of wing
C_N	normal-force coefficient, $\frac{\text{Normal force}}{qS}$
C_A	axial-force coefficient, $\frac{\text{Axial force}}{qS}$
C_L	lift coefficient, $\frac{\text{Lift}}{qS}$
C_D	drag coefficient, $\frac{\text{Drag}}{qS}$
C_Y	side-force coefficient, $\frac{\text{Side force}}{qS}$

C_m pitching-moment coefficient, $\frac{\text{Pitching moment}}{qS\bar{c}}$

C_n yawing-moment coefficient, $\frac{\text{Yawing moment}}{qSb}$

C_l rolling-moment coefficient, $\frac{\text{Rolling moment}}{qSb}$

$C_{Y_\beta} = \frac{\Delta C_Y}{\Delta\beta}$

$C_{n_\beta} = \frac{\Delta C_n}{\Delta\beta}$

$C_{l_\beta} = \frac{\Delta C_l}{\Delta\beta}$

$\beta \approx 0^o, -5^o; \quad \Delta\beta \approx 5^o$

d model body diameter

e wing moment arm about moment reference center

L/D lift-drag ratio

l overall length of model

p_t stagnation pressure

q free-stream dynamic pressure

r radial coordinate

S wing planform area (reference dimension)

S_c canard planform area (including that portion inside fuselage)

t maximum thickness of airfoil section

t/c section thickness ratio

T_t	stagnation temperature
V_∞	free-stream velocity
x	longitudinal coordinate measured rearward from nose of model
x_{cg}	longitudinal distance of moment reference center from model nose
α	angle of attack (referenced to fuselage center line)
δ	canard deflection angle relative to fuselage center line, positive in same sense as α
β	angle of sideslip

Subscripts:

max	maximum
w	wing
c	canard
o	condition evaluated at $\alpha = 0$
r	root
t	tip

For the sake of brevity, especially on the figures, the following code has been devised to designate the various configurations. The letter W denotes the wing and the subscript on W, the wing position on the fuselage. The letter B denotes the nose-fuselage combination and the subscript on B, the body length (canard moment arm). The letter C denotes the canard surface and the subscript on C, the particular canard. (See table I.)

MODEL

Drawings of the model showing dimensions and component arrangements are presented in figure 1. Figure 2 presents the dimensions of the canard control surfaces which were tested. Other pertinent dimensions are presented in table I. Figure 3 presents photographs of two of the configurations tested, and a planview photograph of the family of model components.

The model wing had a 70° swept-leading-edge delta planform with a diamond airfoil section of 5-percent thickness ratio (t/c = 0.05) in the longitudinal direction. The wing was tested in both high and low positions with regard to the fuselage. (See fig. 1.)

The fuselage consisted basically of a circular cylinder afterbody, combined with a sharp 2/3-power nose. The fuselage cylinder was modified in the wing attachment region in order to intersect the wing with essentially flat sides normal to the planform plane. The forward portion of the fuselage could be varied in length by insertion of a 1.200-inch (3.05 cm) cylindrical spacer just ahead of the wing. Figures 1(a) and 3(a) show the model with this spacer in, whereas figures 1(b) and 3(b) show the model with the spacer removed.

Two canard-surface planforms, each with two different areas, were tested: a delta planform with 45° leading-edge sweep, and a trapezoidal planform with 22.5° leading-edge sweep (midchord line unswept). The airfoils for both planforms were sharp-leading-edge 5-percent-chord-thick diamond sections.

The larger delta canard had a total planform area of 19.42 percent of the wing reference area and the smaller, a total area of 14.53 percent of the reference area. For the larger and smaller trapezoidal canards, the areas were 19.32 percent and 14.45 percent, respectively, of the wing reference area. The canard hinge line (fig. 1) was maintained at the same fixed distance from the model nose in all tests.

Vertical tails of trapezoidal planform with 45° swept leading edges were mounted 2.000 inches (5.08 cm) (approximately 80 percent of the wing semispan) from the body center line. The tails also had 5-percent-chord-thick sharp-leading-edge diamond airfoil sections.

TESTS

The tests were made in the Langley 15-inch hypersonic flow apparatus at a Mach number of 10.03. For most of the test runs, the nominal stagnation pressure and temperature were 1000 psia $(6895\ kN/m^2)$ and 1400° F (1033° K), respectively, and resulted in a dynamic pressure of 1.7 psia $(12\ kN/m^2)$ and a Reynolds number per foot of 1.5×10^6 (Reynolds number per meter of 4.92×10^6). For the remainder of the tests, the nominal stagnation pressure and temperature were 800 psia $(5510\ kN/m^2)$ and 1100° F (866° K),

respectively, and yielded a dynamic pressure of 1.3 psia $(9.2\ kN/m^2)$ and the same Reynolds number per foot (1.5×10^6) as for the higher stagnation temperature. The stagnation temperature for the latter runs was reduced in order to alleviate the excessive load on the tunnel heater. Stagnation pressure was reduced at the same time in order to maintain the Reynolds number the same as that for the initial runs. Although operation of the tunnel at the lower values of stagnation temperature and pressure was in a region where air condensation should theoretically exist, an investigation showed that no effective condensation existed at the test conditions. Some of the details of this study of condensation effects are presented in reference 6. Additional details of the basic tunnel characteristics appear in reference 7.

The tests were conducted through an angle-of-attack range of -4^o to 20^o. For each of the two wing vertical positions and each of the two fuselage lengths, the model was tested without the canard and with each of the four canard surfaces at deflection angles of 0^o, 5^o, 10^o, and 20^o. Selected configurations were tested through an angle-of-attack range of -4^o to 20^o at a sideslip angle of -5^o and through a sideslip range of $\beta = -9^o$ to 3^o at zero angle of attack. Also, some runs were made to investigate the effect of vertical tails on both the longitudinal and lateral characteristics of two configurations. Table II presents a listing of the various configurations and the tunnel conditions under which they were tested.

The model was sting-mounted through the fuselage base, and force and moment measurements were made with an internally mounted water-cooled six-component strain-gage balance. Base pressure measurements were not made. The angle of attack and sideslip angle were corrected for sting and balance deflections caused by aerodynamic loads. Angle of attack and sideslip angle are estimated to be accurate within $\pm 0.1^o$.

The estimated maximum errors in the force and moment coefficients, based on a balance accuracy of one-half of one percent of the balance load limits, are as follows:

C_L	± 0.02
C_D	
At an angle of attack of 0^o	± 0.003
At an angle of attack of 20^o	± 0.01
C_Y	± 0.003
C_m	± 0.007
C_l	± 0.0007
C_n	± 0.001

It will be noted that the lift-coefficient scale (0.05 per inch) used on the basic-data plots is somewhat larger than would normally be warranted by the quoted test accuracy.

This expanded scale was used to provide figures of a convenient shape. Because of an inadequately compensated effect of balance heating on normal force resulting in a wind-off zero shift, however, this expanded scale introduces a small spurious effect in the curves for the variation of angle of attack with lift coefficient. On each plot, therefore, there appears to be a small positive lift at zero angle of attack for the canard-off and zero-canard-deflection configurations. This increment in lift coefficient, which is less than the quoted possible balance error, is due to the temperature effect and should be ignored.

Mach number is not measured for each test. The Mach number distribution through the test section (ref. 7) shows a maximum deviation of ± 0.2 from the average Mach number of 10.03.

PRESENTATION OF RESULTS

The basic longitudinal aerodynamic characteristics of the various configurations are presented in figures 4 to 19. The configurations are listed in table II with their corresponding data figure numbers and test conditions. Each of the basic-data figures also includes the data for the corresponding configuration without the canard. Figure 20 presents the effect of wing position on the C_m and C_L curves for selected pairs of configurations. Figures 21 and 22 present the effect of canard size on the C_m curves of selected configurations, both from the point of view of a common moment reference center and from the point of view of a common static margin at $C_L = 0$ and $\delta = 0$. Figure 23 presents the effect of canard planform shape on the C_m curves of two typical configurations. Figure 24 presents the effect of body length (canard moment arm) on the C_m curves of two typical configurations. Figures 25, 26, 27, and 28 present the effects of canards, vertical tails, and wing vertical position on the lateral and directional stability characteristics of a few of the configurations.

RESULTS AND DISCUSSION

Longitudinal Aerodynamic Characteristics

General trends.- The C_L and C_m curves of the canard configurations (figs. 4 to 19) are nonlinear and basically similar in shape for all the configurations tested. The lift-curve slope increases considerably with increasing angle of attack. The C_m curves are typically nonlinear in such a way that the stability level at a given low C_L decreases with increasing canard deflection, and the stability level at a given canard deflection generally increases with increasing C_L above $\alpha = 0^\circ$ to 10° for $\delta = 0^\circ$ to 20°. These typical nonlinearities of the C_m and C_L curves are qualitatively predicted by Newtonian impact theory. The application of impact theory to a skeleton configuration

(fig. 29) consisting of two flat plates of the proper relative surface areas at the proper relative angles and distances is presented in an appendix. A comparison of the theoretical curves of figure 30 with the canard configuration data of figures 4 to 19 shows that the nonlinearities of the C_m and C_L curves, which are common to all the canard configurations, are inherent in the hypersonic flow regime.

At a given C_L, C_D increases, as would be expected, with a canard deflection from 0^o to 20^o, and there is an accompanying loss in $(L/D)_{max}$ of 0.5 to nearly 1.0. For the lesser canard deflections, the drag increment is dependent on the configuration parameters. (See figs. 4 to 19.)

Effects of wing position.- With the canard off, there is little difference between the lift-curve slopes of the high-wing (figs. 4 to 11) and low-wing (figs. 12 to 19) configurations. With the canards on, there is generally an increase in C_{L_o} with increasing δ for both wing positions. For the low-wing configurations, the lift-curve slope is generally about constant with increasing canard deflection at a given angle of attack, as predicted by impact theory (fig. 30), whereas for the high-wing configurations the lift-curve slope tends to decrease with increasing canard deflection. Thus, at the highest angles of attack, C_L for the low-wing configurations increases with increasing δ as at the lower angles of attack, whereas C_L for the high-wing configurations increases only slightly or not at all. (See fig. 20.) As a result of this loss in lift on the high-wing configurations, compared with the low-wing configurations, the high-wing configurations have a positive increment in C_m at the higher angles of attack and canard deflection. This result obviously indicates that the loss in lift occurs behind the moment reference center. These effects of wing position are due to a much greater interference of the canard on the high-wing configurations than on the low-wing configurations. It is probably caused by the low pressure field above the canard acting on the underside of the high wing. As a result of this canard-wing interference, the canard is a more powerful trimming device on the high-wing configurations than on the low-wing configurations.

A comparison of the C_D curves for the high-wing configurations (figs. 4 to 11) with those of the low-wing configurations (figs. 12 to 19) shows that there is no significant difference due to wing position on the C_D curves for $\delta = 0$. However, C_D increases more rapidly with canard deflection at a given high C_L on the high-wing configurations than on the corresponding low-wing configurations. This effect is due to the fact that the high-wing configurations require a greater α to attain a given C_L than the low-wing configurations.

Effects of canard size.- The canard-wing area ratio of the large canards is nominally one-third greater than that of the small canards. (See fig. 2.) The C_m curves of two pairs of typical configurations (figs. 21(a) and 22(a)) show that, as would be expected, the large-canard configurations are less longitudinally stable than the corresponding

small-canard configurations. If the moment reference center locations of the large-canard configurations are adjusted so that these configurations have the same static margin at $C_L = 0$ and $\delta = 0$ as the small-canard configurations, it can be seen directly (figs. 21(b) and 22(b)) that the large canards are more effective than the small canards. The comparison of the C_m curves for the large-canard configuration with those for the small-canard configuration having a common static margin at $C_L = 0$ and $\delta = 0$ (fig. 21(b)) also shows that the greater effectiveness of the larger canard on the high-wing configuration is primarily due to an increase in C_{m_o} with little change in the stability. On the low-wing configuration (fig. 22(b)), on the other hand, there is primarily a greater decrease in stability level with increasing C_L for the large-canard configuration than for the small-canard configuration (in spite of the common static margin at $C_L = 0$ and $\delta = 0$), and this decrease is accompanied by little or no change in C_{m_o}.

Effects of canard planform shape.- Since any effect of canard shape on the aerodynamic characteristics of the configurations would be expected to increase with canard size and body length (canard moment arm), direct comparisons of the delta and trapezoidal canards are presented for the large-canard long-body configurations. (See fig. 23.) With $\delta = 0$, the effect of canard planform shape is negligible for both the high-wing configurations (fig. 23(a)) and the low-wing configurations (fig. 23(b)). It appears, however, that the trapezoidal canard is more effective than the delta canard in view of the more positive values of C_m for the trapezoidal canard configurations at the higher canard deflections and lift coefficients for both wing positions.

Effects of body length.- For a common moment reference center location of 60 percent of the body length, the long-body B_2 and short-body B_1 configurations do not have the moment reference center in the same position relative to the wing. However, since the effect of body length on the C_m curve for $\delta = 0$ is negligible (fig. 24), the configurations may be compared on the basis of a common static margin at $\delta = 0$ without any adjustment in moment reference center location. The configurations presented in figure 24 are typical of the others for which data are available. It would be expected that the canard control would be more effective on the long-body configurations than on the corresponding short-body configurations. For the high-wing configuration (fig. 24(a)), the greater effectiveness of the canard on the long body is significant at $\delta = 10^\circ$ and $\delta = 20^\circ$ and for the low-wing configuration only at $\delta = 20^\circ$. It appears that this greater effectiveness of the canard on the longer body configuration at the higher values of δ is mainly due to an increase in C_{m_o} caused by the increased moment arm of the canard rather than any change in canard interference on the wing, since the effects are similar for both the high-wing and low-wing configurations.

Lateral and Directional Stability Characteristics

Effects of canards.- The data of figure 25 for the high-wing long-body small-canard configurations show that with or without the canards and with the canard (C_1 or C_3) deflected 10^o, C_l, C_n, and C_Y vary linearly with β at $\alpha = 0$ in the sideslip angle range of these tests. Thus, the ensuing data, showing stability derivatives through the angle-of-attack range, may be interpreted as being both quantitatively and qualitatively valid. It is assumed that a difference in wing position, body length, canard size, or angles of attack other than 0^o will not materially affect the linearity of the lateral and directional characteristics.

The presence of the canard and canard deflection to 10^o has no significant effect on the lateral and directional coefficients or stability derivatives for angles of attack near 0^o. The presence of the canard reduces the directional stability slightly (fig. 26), tail-off or tail-on, at angles of attack above about 8^o, on the high-wing configurations, but there is no significant additional effect of canard deflection. For the low-wing configuration, with the vertical tails on (fig. 27(c)), the presence of the canard increases the directional stability slightly above $\alpha = 6^o$, but canard deflection from 0^o to 10^o reduces the stability to about the canard-off level.

The dihedral effect is slightly reduced by the presence of the canards on the high-wing configurations, tail-off or tail-on (figs. 27(a) and 27(b)). On the low-wing configurations, however, with the vertical tail on (fig. 27(c)), for $\alpha > 12^o$, the presence of the canard increases the dihedral effect considerably, whereas deflection of the canard from 0^o to 10^o reduces the positive dihedral to the canard-off level.

Effects of vertical tails.- The effect of vertical tails on directional stability (fig. 27), as would be expected, is to increase directional stability in the angle-of-attack range investigated for both the low-wing configuration and the high-wing configurations.

The dihedral effect of the vertical tails on the canard configurations is dependent on canard planform (fig. 27). For the high-wing, long-body, small-delta-canard configuration $W_1B_2C_1$ (fig. 27(a)), the vertical tails give more positive dihedral at low angles of attack, or with the canard off. Above an angle of attack of about 5^o with the canard on, the effect is reversed. For the high-wing long-body small-trapezoidal-canard configuration, the vertical tails increase the positive dihedral up to an angle of attack dependent on the canard deflection, above which the effect vanishes (fig. 27(b)). The vertical tails generally have little effect on the dihedral of the low-wing configuration $W_2B_2C_1$ (fig. 27(c)) except for a sharp increase in positive dihedral due to the vertical tails for the $\delta = 0$ condition and $\alpha > 12^o$.

Effects of wing position.- Figure 28 shows that the high-wing configurations have better directional stability and higher positive dihedral effect than the corresponding

low-wing configurations tested with or without the canards or vertical tails. This effect of wing position probably results from the fact that as angle of attack increases, the sides of the body are increasingly in the hypersonic "shadow region" created by the bottom-mounted wing; thus, the available restoring moment necessary for stability is greatly reduced.

SUMMARY OF RESULTS

An experimental investigation has been made in the Langley 15-inch hypersonic flow apparatus at a Mach number of 10.03 to determine the effects of canard size, canard planform, body length, wing position, and vertical tails on the longitudinal and lateral aerodynamic characteristics of a high-fineness-ratio canard-control configuration with a 70°-swept delta wing. The results indicate:

1. As predicted by Newtonian impact theory, lift-curve slope increases with angle of attack, and the pitching-moment coefficient is nonlinear in such a way that the stability level decreases sharply with canard deflection at low lift coefficients and increases with lift coefficient for a given canard deflection at the higher lift coefficients.

2. The lower total lift and greater effectiveness of the canard on the high-wing configurations as compared with the corresponding low-wing configurations probably result from interference of the canard wake and/or shock field with the flow under the wing.

3. The trapezoidal canard is somewhat more effective than the delta canard, although the difference in effectiveness is negligible for low canard deflections and low lift coefficients.

4. For the high-wing configurations, the canard is more effective on the long body than on the short body, whereas for the low-wing configurations, the difference is slight except for the highest canard deflection.

5. The variation of the lateral and directional coefficients with sideslip angle appears to be linear at zero angle of attack, although only two configurations were tested through a range of sideslip angle. The effects of canard presence and deflection on the lateral and directional stability are negligible except at the higher angles of attack, where some configuration-dependent variations occur.

6. The dihedral effect of the vertical tails is somewhat less on the low-wing configurations than on the high-wing configurations.

7. The high-wing configurations are more laterally and directionally stable than the corresponding low-wing configurations, probably because the rearward sides of the body are in the hypersonic shadow region created by the bottom-mounted wing.

Langley Research Center,
National Aeronautics and Space Administration,
Langley Station, Hampton, Va., January 6, 1966.

APPENDIX

QUALITATIVE PREDICTION OF CANARD CONFIGURATION CHARACTERISTICS BY MEANS OF NEWTONIAN IMPACT THEORY

The characteristic variation of α and C_m with C_L for a canard control configuration can be shown (qualitatively) by the application of Newtonian impact theory to a simple skeleton configuration in which the wing and canard surfaces are represented by flat plates of proper area ratio. (See fig. 29.) The canard-wing area ratio $\frac{S_c}{S}$ is taken as 0.20 for the present illustration; this value closely matches the area ratios of the large delta and trapezoidal canards of the present tests, which are 0.1942 and 0.1932, respectively. The canard moment arm a is taken as the distance between the moment reference center and the canard hinge line for the long-nose B_2 configurations (a = 4.746 in. (12.05 cm)). (See fig. 1.) The wing moment arm e is taken as the distance from the moment reference center to the centroid of area of the wing planform for the long-nose B_2 configurations (e = 2.466 in. (6.26 cm)). If the lift- and pitching-moment coefficients are referenced to the wing planform area S and wing mean aerodynamic chord $\bar{c}$ the following relations may be written for the wing:

$$C_{N,w} = 2 \sin^2\alpha$$

$$C_{A,w} = 0$$

$$C_{L,w} = C_{N,w} \cos\alpha - C_{A,w} \sin\alpha$$

$$C_{m,w} = -C_{N,w}\left(\frac{e}{\bar{c}}\right)$$

As a result,

$$C_L = 2 \sin^2\alpha \cos\alpha$$

$$C_m = -2\left(\frac{e}{\bar{c}}\right)\sin^2\alpha$$

Similarly, the following relations exist for the canard:

$$C_{N,c} = 2 \frac{S_c}{S} \sin^2(\alpha + \delta)$$

$$C_{A,c} = 0$$

APPENDIX

$$C_{L,c} = C_{N,c} \cos(\alpha + \delta) - C_{A,c} \sin(\alpha + \delta)$$

$$C_{m,c} = C_{N,c} \frac{a}{\bar{c}} \cos \delta$$

As a result,

$$C_L = 2 \frac{S_c}{S} \sin^2(\alpha + \delta)\cos(\alpha + \delta)$$

$$C_m = 2 \frac{S_c}{S} \frac{a}{\bar{c}} \sin^2(\alpha + \delta)\cos \delta$$

Thus, for the total skeleton configuration,

$$C_L = 2 \sin^2\alpha \cos \alpha + 2 \frac{S_c}{S} \sin^2(\alpha + \delta)\cos(\alpha + \delta)$$

$$C_m = 2 \frac{e}{\bar{c}} \sin^2\alpha + 2 \frac{S_c}{S} \frac{a}{\bar{c}} \sin^2(\alpha + \delta)\cos \delta$$

Figure 30 shows a plot of these equations using the same scales as for the basic experimental data, and the values of a, d, and $\frac{S_c}{S}$ previously given. These theoretical curves closely match the general shapes of the experimental curves for the low-wing long-nose large-canard configurations, $W_2B_2C_2$ and $W_2B_2C_4$, and indicate that the nonlinearities of the experimental data are inherent characteristics of the hypersonic flow regime.

REFERENCES

1. Hall, Charles F.; and Boyd, John W.: Effects of Canards on Airplane Performance and Stability. NACA RM A58D24, 1958.

2. Spearman, M. Leroy; and Driver, Cornelius: Some Factors Affecting the Stability and Performance Characteristics of Canard Aircraft Configurations. NACA RM L58D16, 1958.

3. Morris, Owen G.; Carmel, Melvin M.; and Carraway, Ausley B.: An Investigation at Mach Numbers From 0.20 to 4.63 of the Aerodynamic Performance, Static Stability, and Trimming Characteristics of a Canard Configuration Designed For Efficient Supersonic Cruise Flight. NASA TM X-617, 1961.

4. Carraway, Ausley B.; Morris, Owen G.; and Carmel, Melvin M.: Aerodynamic Characteristics at Mach Numbers From 0.20 to 4.63 of a Canard-Type Supersonic Commercial Air Transport Configuration. NASA TM X-628, 1962.

5. Putnam, Lawrence E.; and Trescot, Charles D., Jr.: Hypersonic Aerodynamic Characteristics of Plain and Ported Elevon Controls on a 75° Swept Modified Delta-Wing Configuration. NASA TM X-987, 1964.

6. Putnam, Lawrence E.: Investigation of Effects of Ramp Span and Deflection Angle on Laminar Boundary-Layer Separation at Mach 10.03. NASA TN D-2833, 1965.

7. Putnam, Lawrence E.; and Brooks, Cuyler W., Jr.: Static Longitudinal Aerodynamic Characteristics at a Mach Number of 10.03 of Low-Aspect-Ratio Wing-Body Configurations Suitable For Reentry. NASA TM X-733, 1962.

TABLE I.- MODEL GEOMETRY AND COMPONENT DESIGNATION CODE

[Wing planform area, S, 17.815 in.^{2} (114.9353 cm^2); wing mean aerodynamic chord, $\bar{c}$, 4.667 in. (11.854 cm); and wing span, b, 5.090 in. (12.9286 cm)]

Component	Dimension	Code designation
Fuselage (including nose):		B
Length (total)	10.800 in. (27.43 cm)	B_1
Length (total	12.000 in. (30.48 cm)	B_2
Diameter, d	1.000 in. (2.54 cm)	
Nose length	3.800 in. (9.65 cm)	
Nose profile	$\frac{r}{d} = 0.2218 \left(\frac{x}{d}\right)^{2/3}$	
Canard control surfaces:		C
Small delta canard:		C_1
Root chord, c_r	1.609 in. (4.087 cm)	
Leading-edge sweep	45°	
Trailing-edge sweep	0°	
Diamond airfoil section thickness ratio, t/c	0.050	
Planform area, S_c	2.589 in.^{2} (16.703 cm^2)	
Area ratio, S_c/S	0.1453	
Large delta canard:		C_2
Root chord, c_r	1.860 in. (4.724 cm)	
Leading-edge sweep	45°	
Trailing-edge sweep	0°	
Diamond airfoil section thickness ratio, t/c	0.050	
Planform area, S_c	3.460 in.^{2} (22.3225 cm^2)	
Area ratio, S_c/S	0.1942	
Small trapezoidal canard:		C_3
Root chord, c_r	1.609 in. (4.087 cm)	
Tip chord, c_t	0.675 in. (1.714 cm)	
Span, b	2.254 in. (5.725 cm)	
Leading-edge sweep	22.5°	
Trailing-edge sweep	22.5°	
Diamond airfoil section thickness ratio, t/c	0.050	
Planform area, S_c	2.574 in.^{2} (16.6064 cm^2)	
Area ratio, S_c/S	0.1445	

TABLE I.- MODEL GEOMETRY AND COMPONENT DESIGNATION CODE - Concluded

Component	Dimension	Code designation
Large trapezoidal canard:		C_4
Root chord, c_r	1.860 in. (4.724 cm)	
Tip chord, c_t	0.780 in. (1.981 cm)	
Span, b	2.608 in. (6.624 cm)	
Leading-edge sweep	22.5°	
Trailing-edge sweep	22.5°	
Diamond airfoil section thickness ratio, t/c	0.050	
Planform area, S_c	3.443 $in.^2$ (22.2129 cm^2)	
Area ratio, S_c/S	0.1932	
Wing:		W
Root chord, c_r	7.000 in. (17.780 cm)	
Span, b	5.090 in. (12.929 cm)	
Mean aerodynamic chord, $\bar{c}$	4.667 in. (11.854 cm)	
Leading-edge sweep	70°	
Trailing-edge sweep	0°	
Diamond airfoil section thickness ratio, t/c	0.050	
Planform area, S	17.815 $in.^2$ (114.9353 cm^2)	
Position on fuselage	High wing	W_1
	Low wing	W_2
Vertical tails:		
Root chord, c_r	1.500 in. (3.810 cm)	
Tip chord, c_t	0.300 in. (0.762 cm)	
Leading-edge sweep	45°	
Trailing-edge sweep	0°	
Diamond airfoil section thickness ratio, t/c	0.050	
Planform area (each)	1.080 $in.^2$ (6.9677 cm^2)	
Area ratio (both)	0.1212	

TABLE II.- TEST CONDITIONS

Configuration	δ, deg	T_t, °F (°K)	p_t, psia (kN/m^2)	Figures in which data are presented
W_1B_1	Canard off	1400 (1033)	1000 (6895)	4, 5, 6, 7
$W_1B_1C_1$	0, 5, 10, 20	1400 (1033)	1000 (6895)	4
$W_1B_1C_2$	0, 5, 10, 20	1400 (1033)	1000 (6895)	5
$W_1B_1C_3$	0, 5, 10, 20	1400 (1033)	1000 (6895)	6
$W_1B_1C_4$	0, 5, 10, 20	1400 (1033)	1000 (6895)	7
W_1B_2	Canard off	1400 (1033)	1000 (6895)	8, 9, 10, 11
W_1B_2	Canard off	1100 (866)	800 (5516)	25 (lateral)
$W_1B_2C_1$	0, 5, 10, 20	1400 (1033)	1000 (6895)	8
$W_1B_2C_1$	0, 10	1100 (866)	800 (5516)	25 (lateral)
$W_1B_2C_2$	0, 5, 10, 20	1100 (866)	800 (5516)	9
$W_1B_2C_3$	0, 5, 10, 20	1100 (866)	800 (5516)	10
$W_1B_2C_3$	0, 10	1100 (866)	800 (5516)	25 (lateral)
$W_1B_2C_4$	0, 5, 10, 20	1100 (866)	800 (5516)	11
W_2B_1	Canard off	1400 (1033)	1000 (6895)	12, 13, 14, 15
$W_2B_1C_1$	0, 5, 10, 20	1400 (1033)	1000 (6895)	12
$W_2B_1C_2$	0, 5, 10, 20	1400 (1033)	1000 (6895)	13
$W_2B_1C_3$	0, 5, 10, 20	1400 (1033)	1000 (6895)	14
$W_2B_1C_4$	0, 5, 10, 20	1400 (1033)	1000 (6895)	15
W_2B_2	Canard off	1400 (1033)	1000 (6895)	16, 17, 18, 19
$W_2B_2C_1$	0, 5, 10, 20	1400 (1033)	1000 (6895)	16
$W_2B_2C_2$	0, 5, 10, 20	1400 (1033)	1000 (6895)	17
$W_2B_2C_3$	0, 5, 10, 20	1400 (1033)	1000 (6895)	18
$W_2B_2C_4$	0, 5, 10, 20	1400 (1033)	1000 (6895)	19

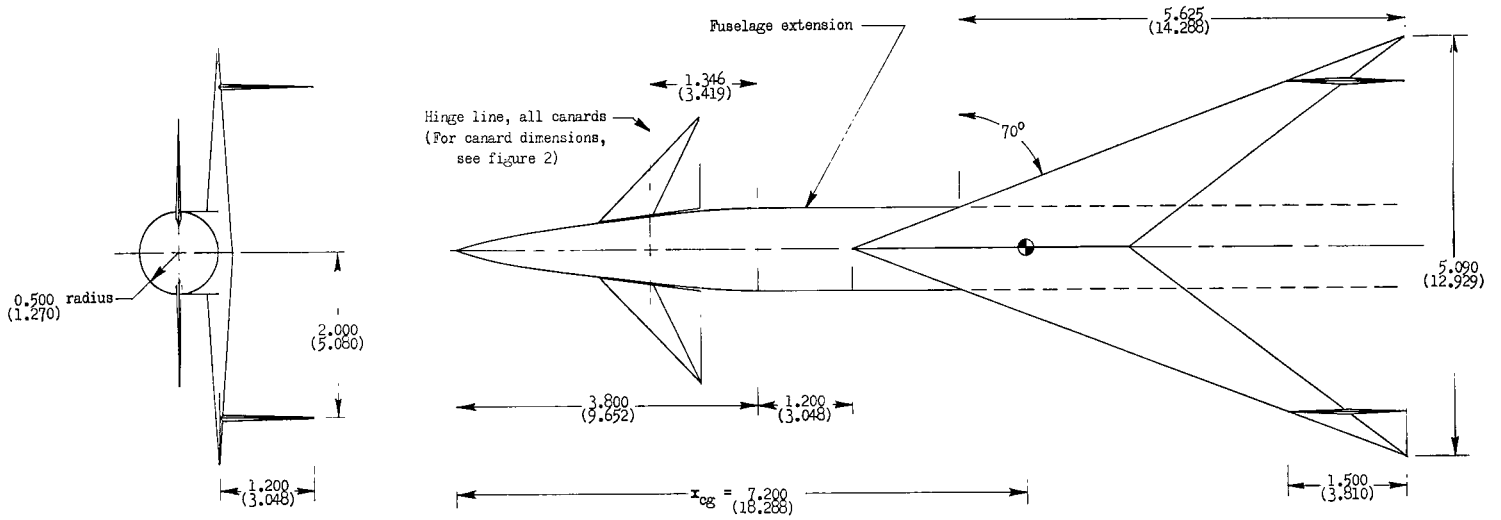

Nose profile

x/d	r/d
0	0
.5	.1397
1.0	.2218
1.5	.2907
2.0	.3520
2.5	.4085
3.0	.4610
3.1	.4710
3.2	.4800
3.3	.4860
3.4	.4915
3.5	.4960
3.6	.4980
3.7	.5000
3.8	.5000

d = 1.000
(2.540)

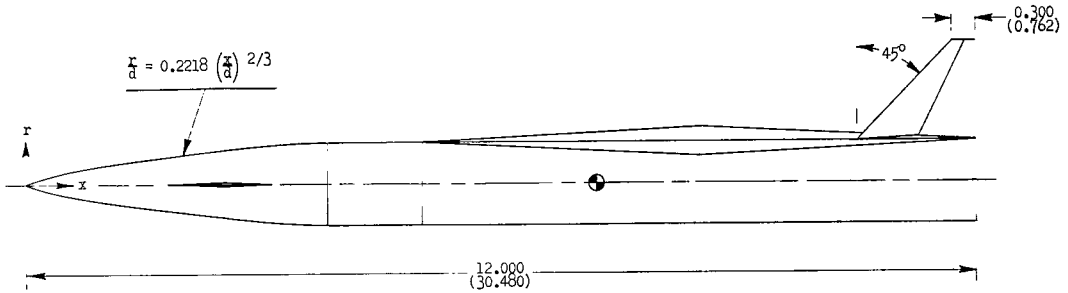

(a) High-wing long-body configuration.

Figure 1.- Model drawings. All dimensions are in inches (cm). All airfoil sections are 0.05-thickness-ratio diamond sections.

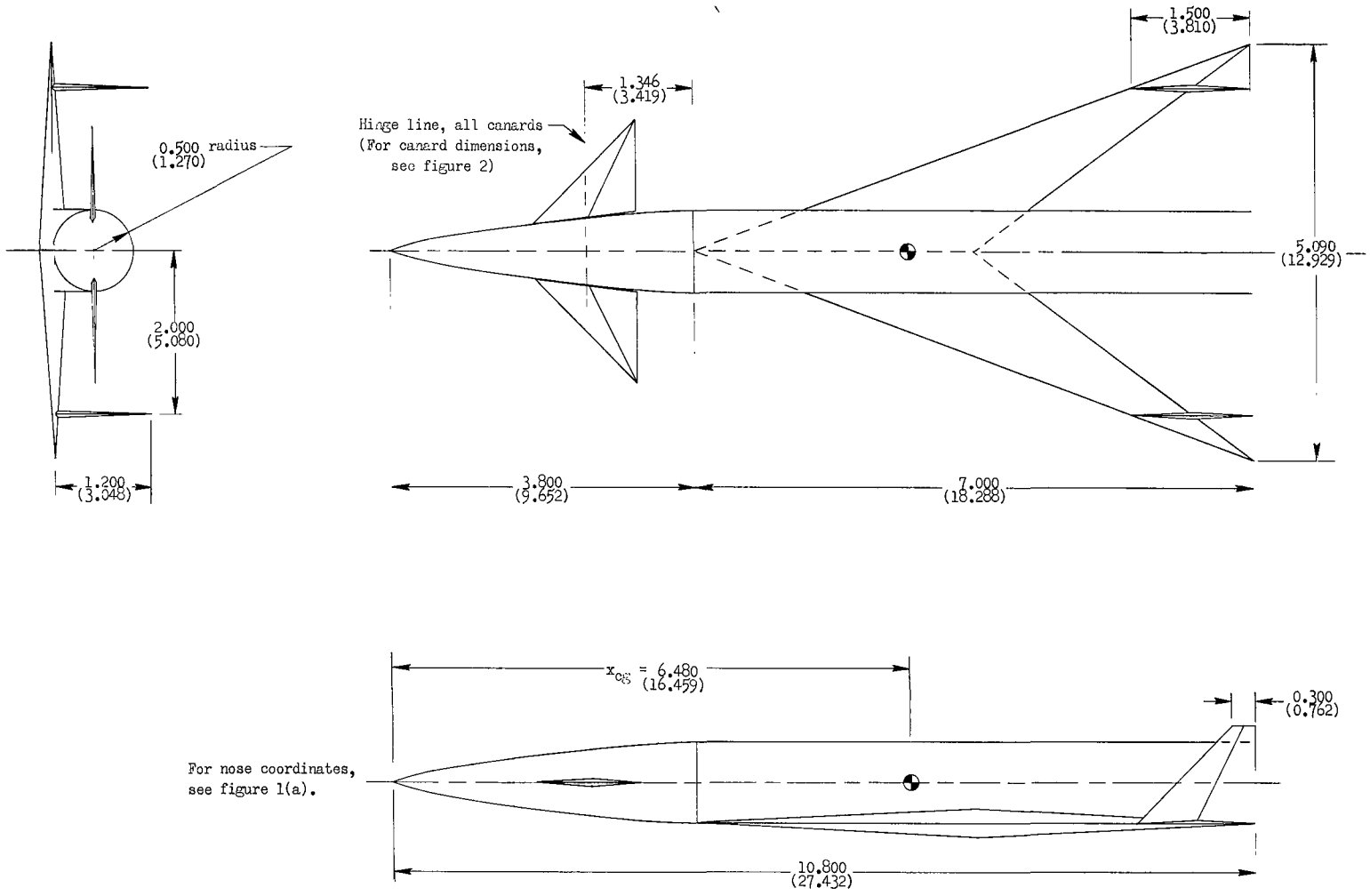

(b) Low-wing short-body configuration.

Figure 1.- Concluded.

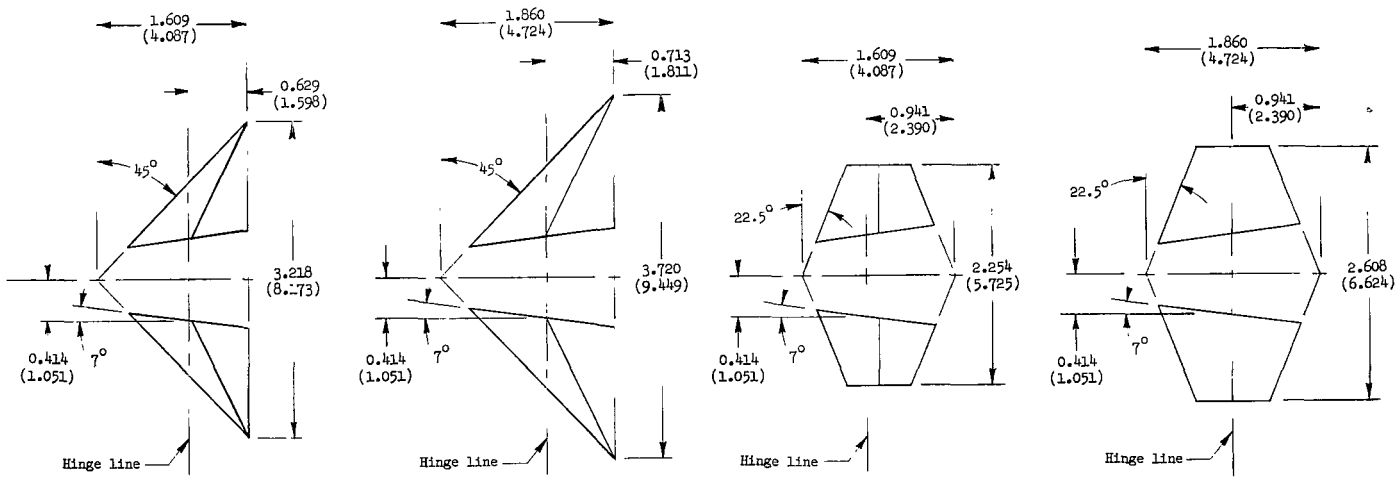

Small delta canard
$S_c/S = 0.1453$

Large delta canard
$S_c/S = 0.1942$

Small trapezoidal canard
$S_c/S = 0.1445$

Large trapezoidal canard
$S_c/S = 0.1932$

Figure 2.- Planform detail of canard control surfaces. All dimensions in inches (cm).

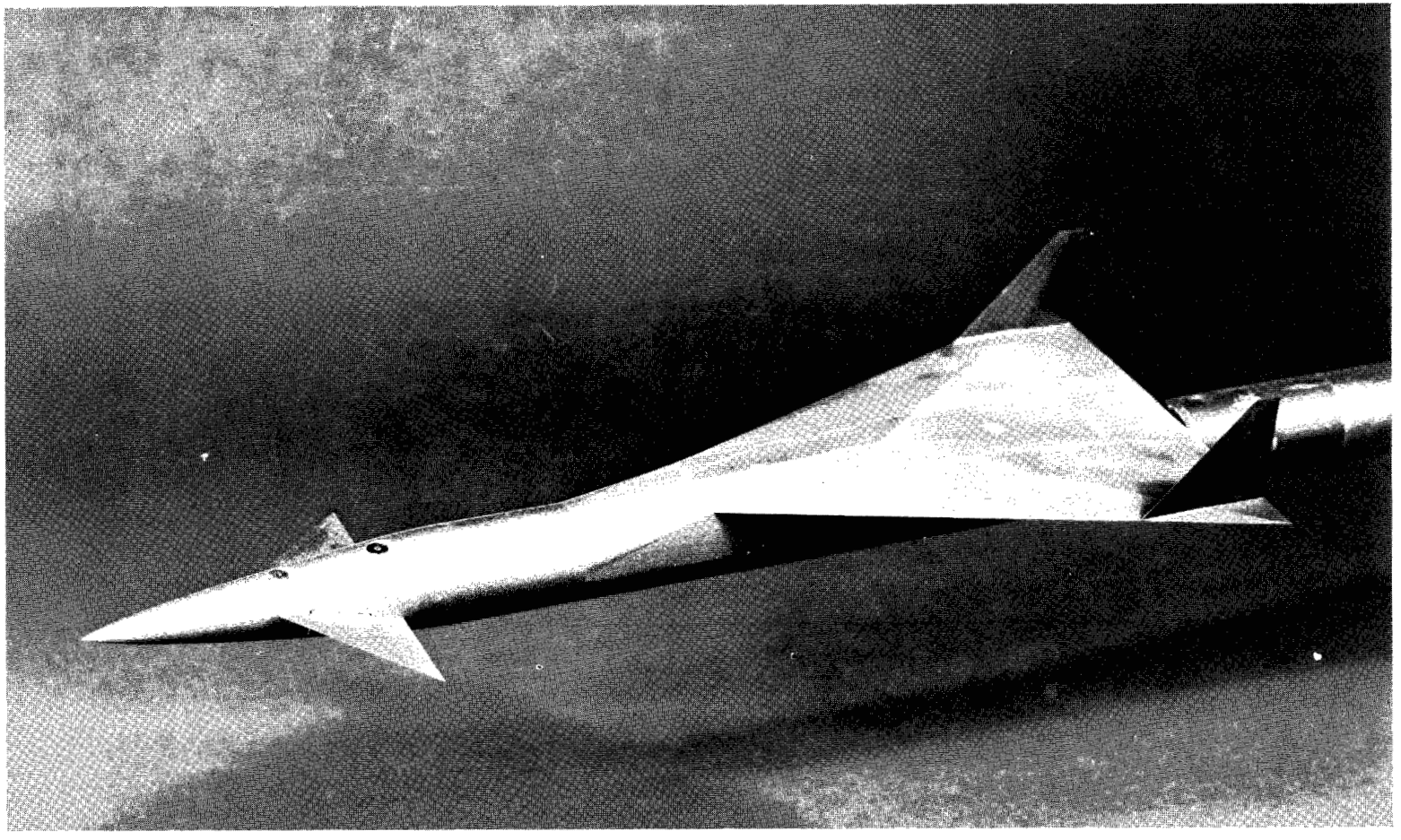

(a) Configuration $W_1B_2C_1$; $\delta = 10^0$.

L-63-9746

Figure 3.- Selected model photographs.

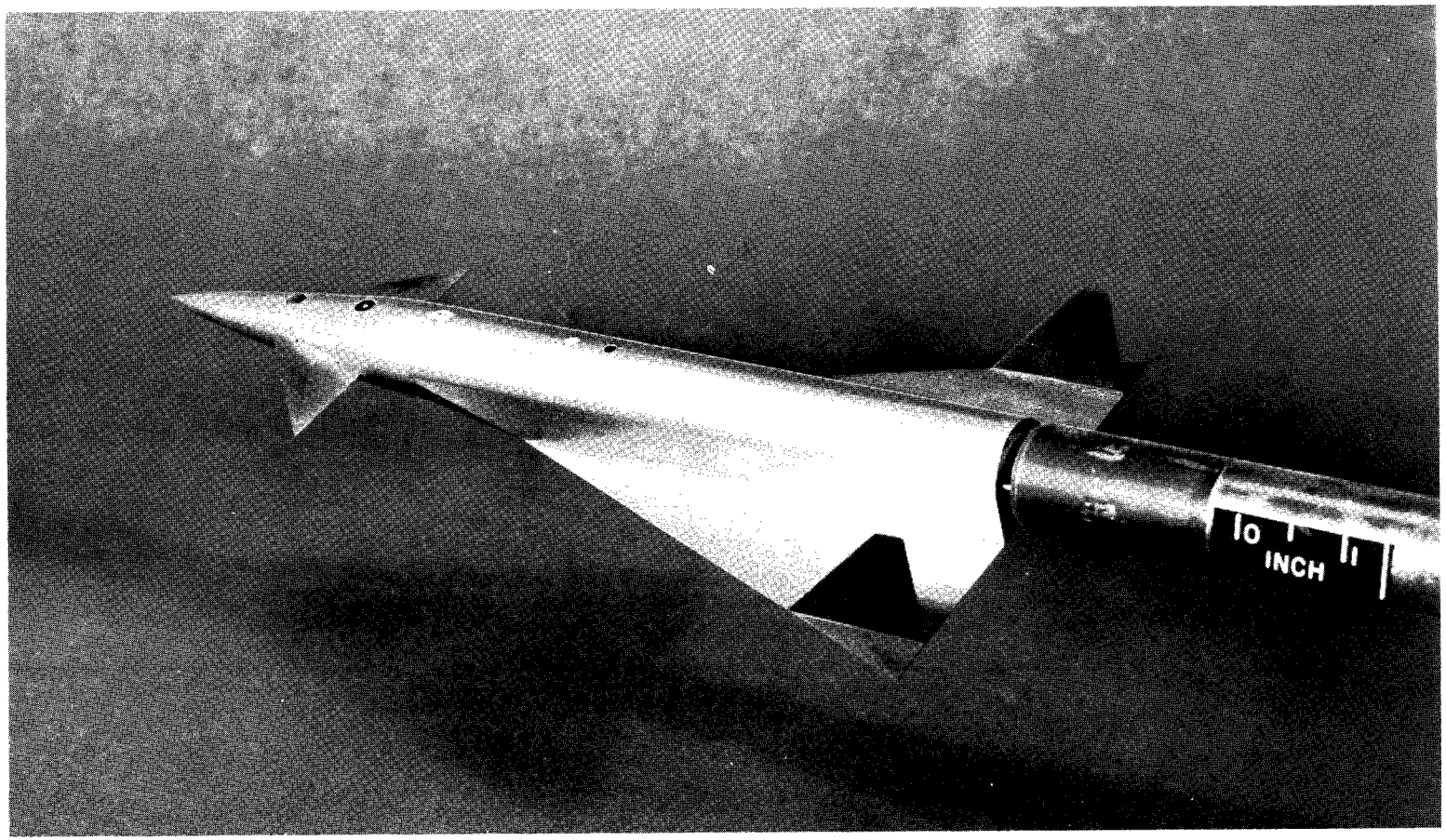

(b) Configuration $W_2B_1C_1$; $\delta = 10^0$. L-63-9743

Figure 3.- Continued.

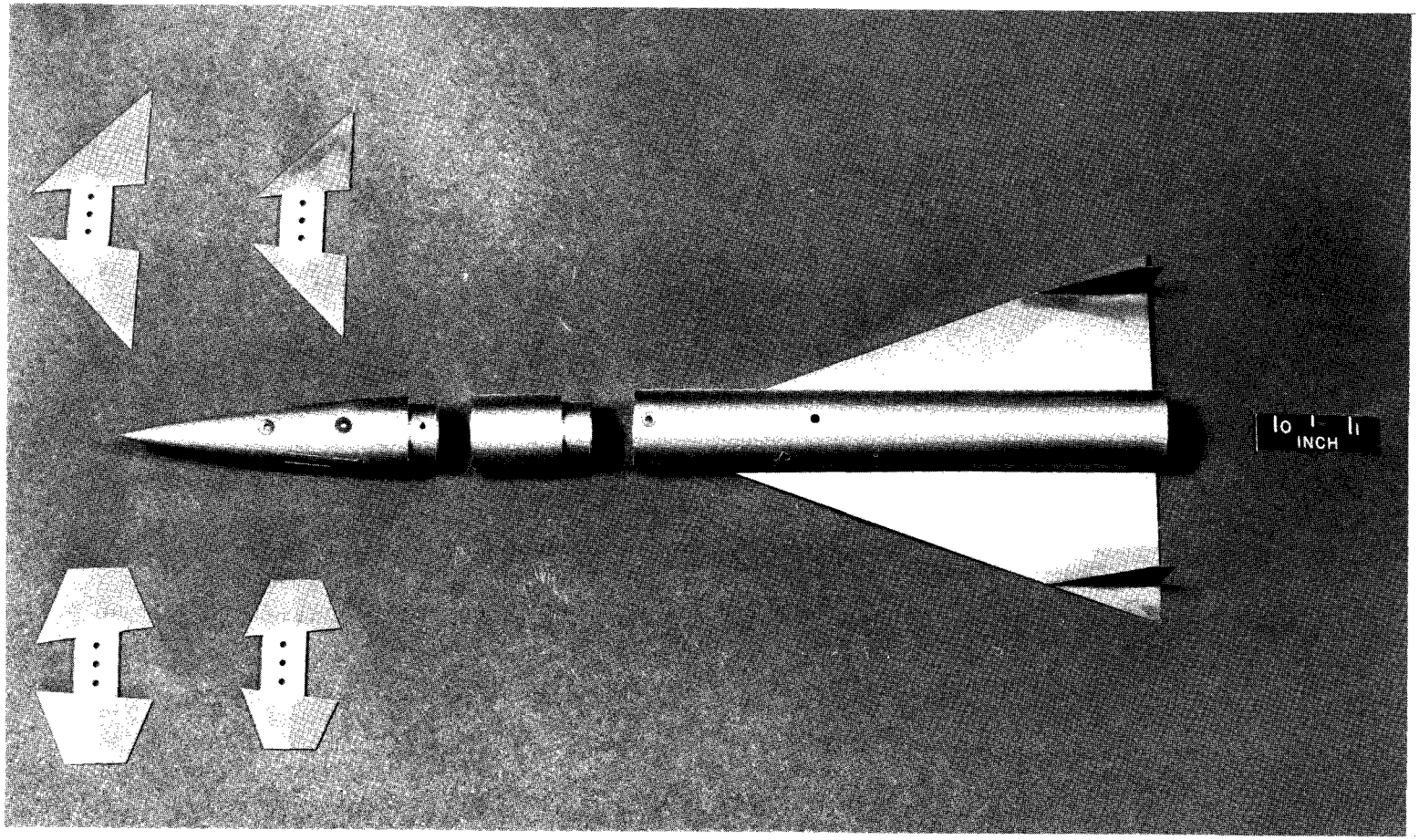

(c) Planform view of all model components. L-63-9744

Figure 3.- Concluded.

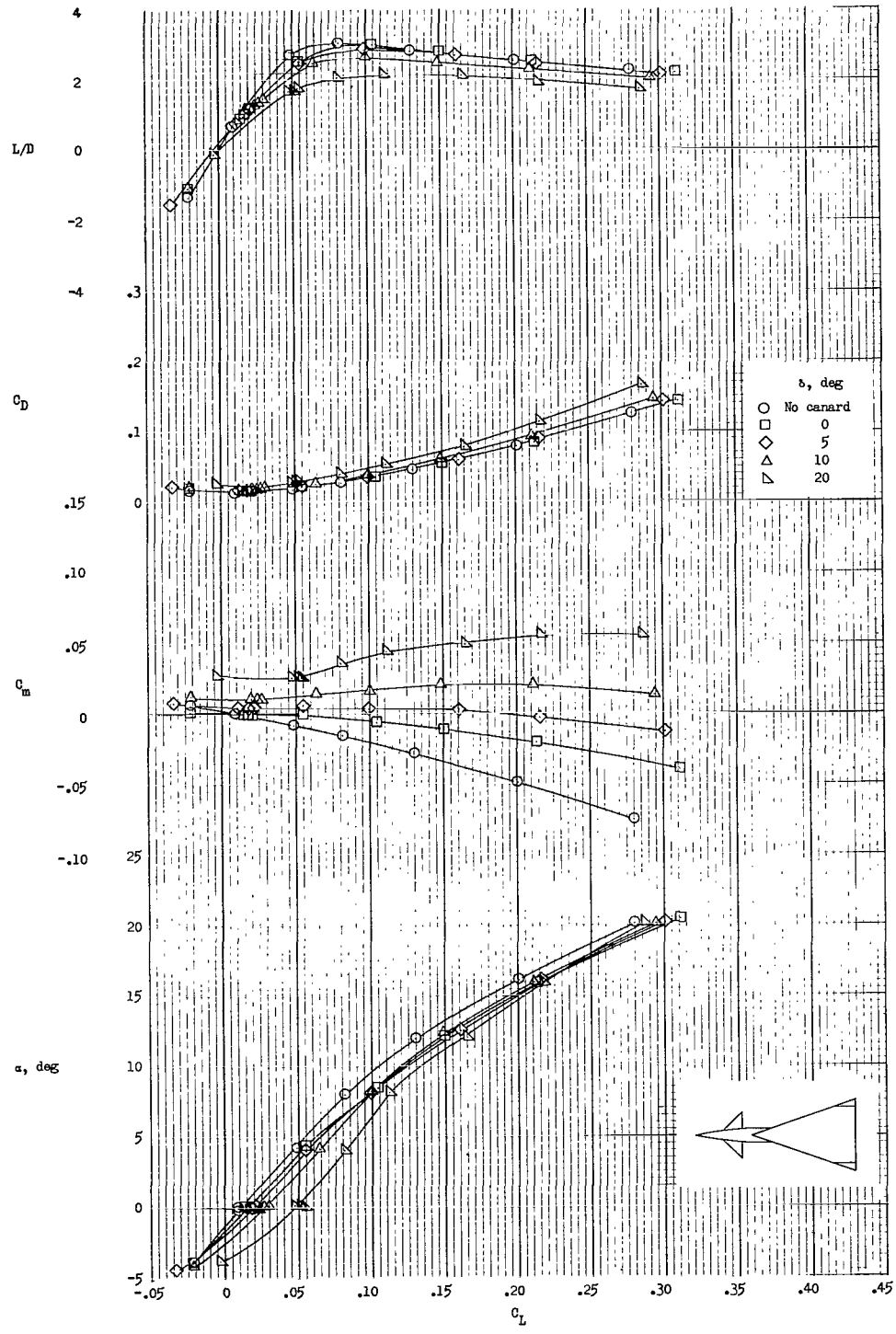

Figure 4.- Longitudinal aerodynamic characteristics of configuration $W_1B_1C_1$ with canard off and with various canard deflections.

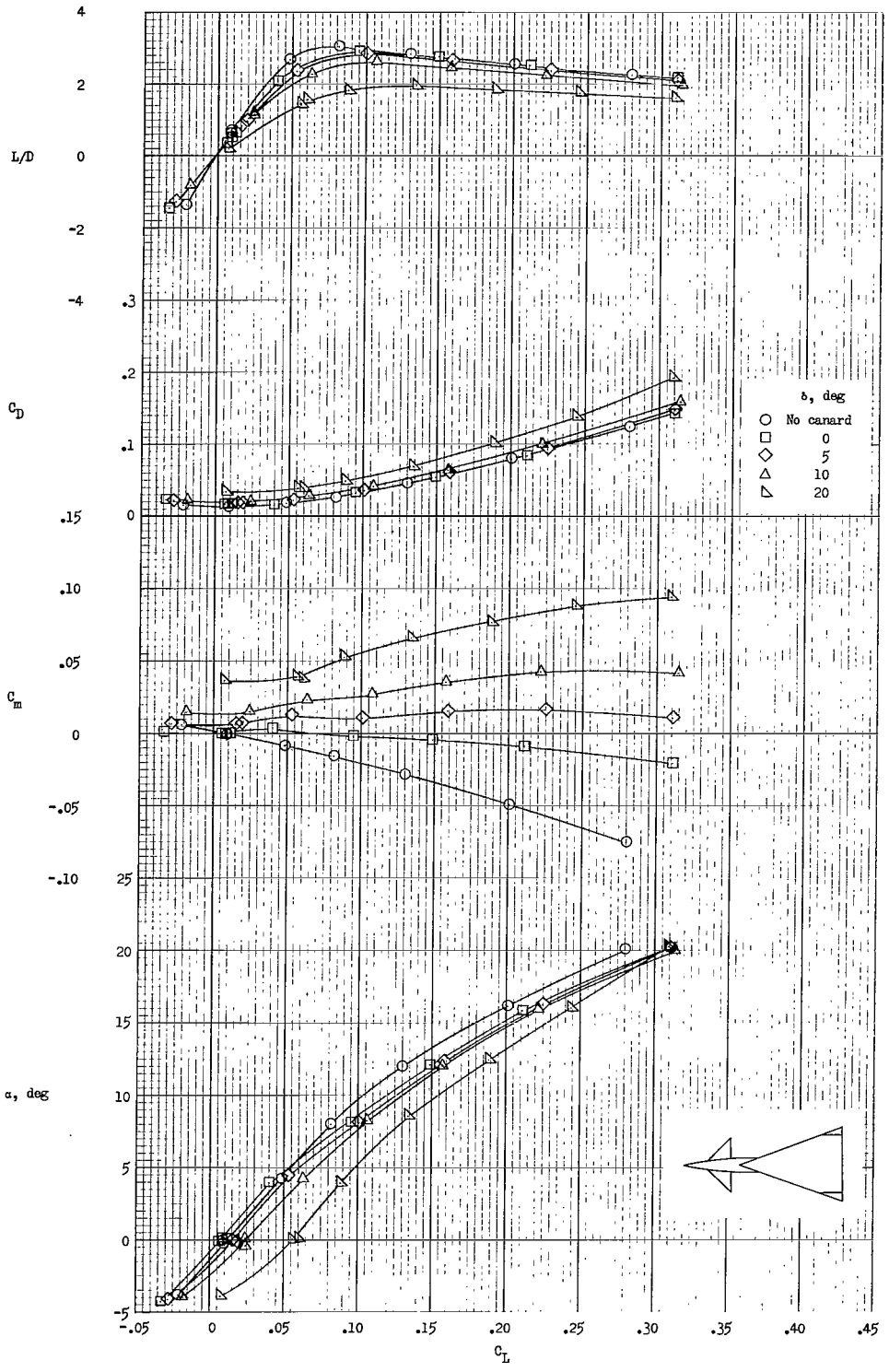

Figure 5.- Longitudinal aerodynamic characteristics of configuration $W_1B_1C_2$ with canard off and with various canard deflections.

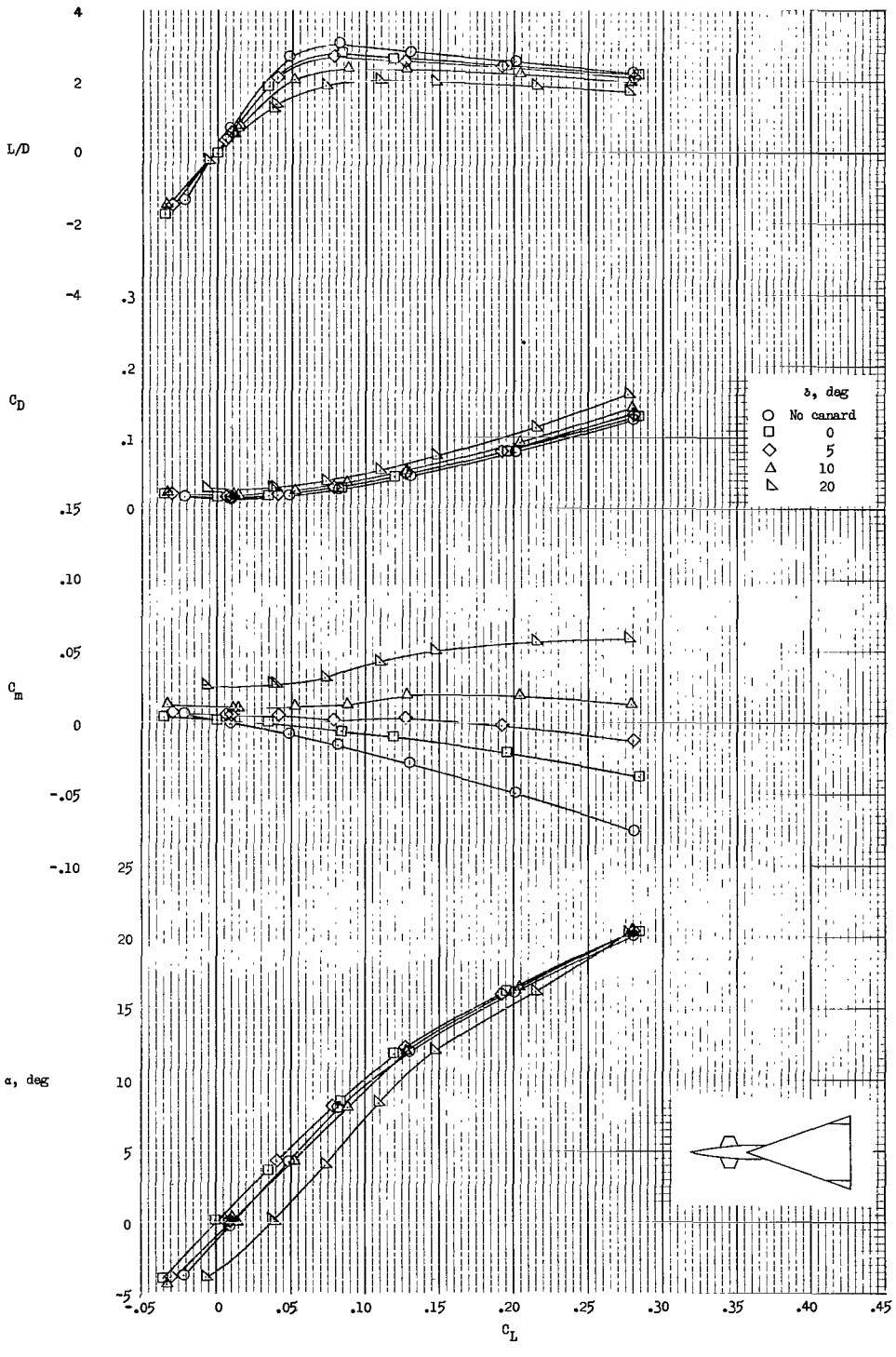

Figure 6.- Longitudinal aerodynamic characteristics of configuration $W_1B_1C_3$ with canard off and with various canard deflections.

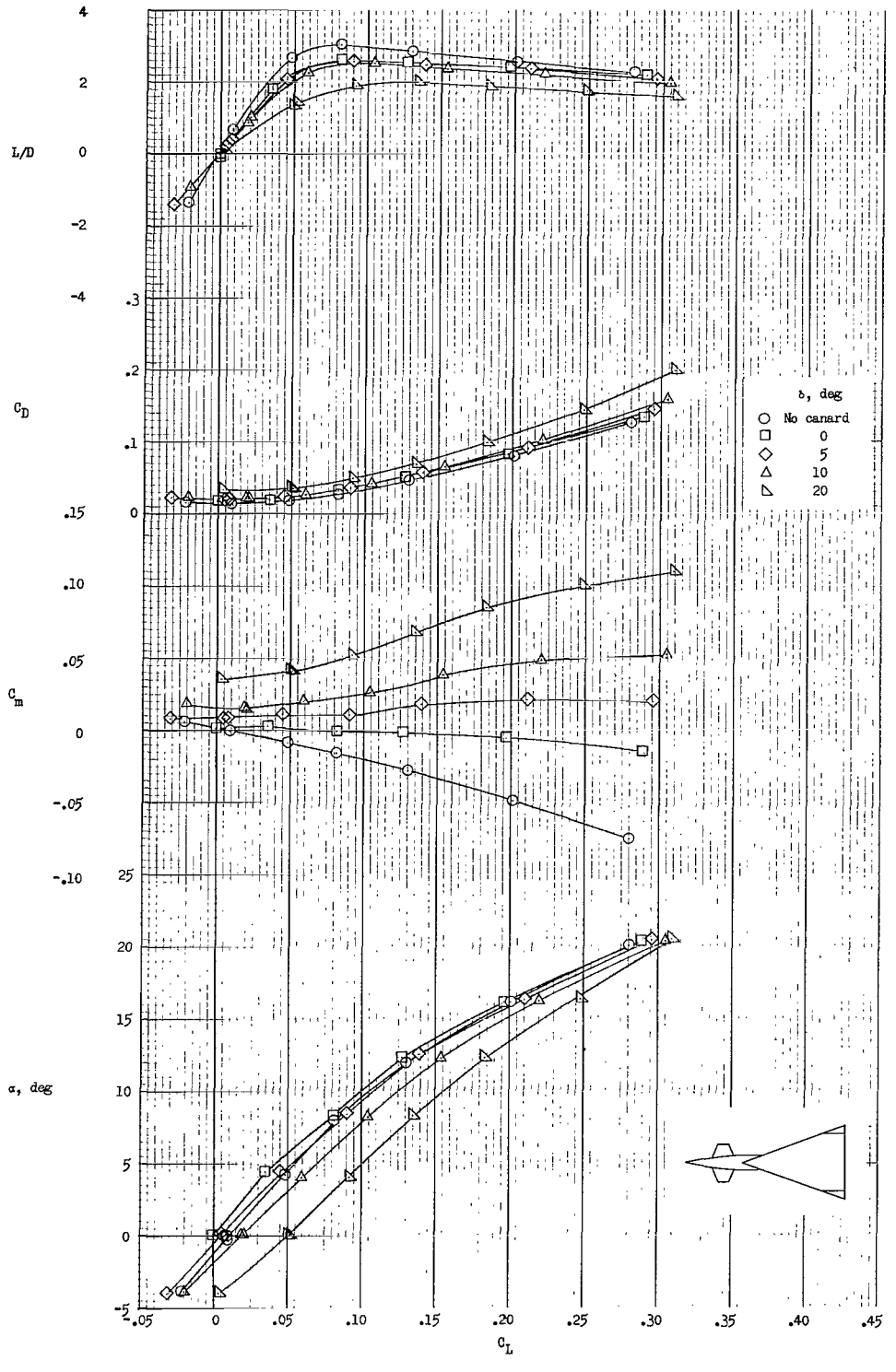

Figure 7.- Longitudinal aerodynamic characteristics of configuration $W_1B_1C_4$ with canard off and with various canard deflections.

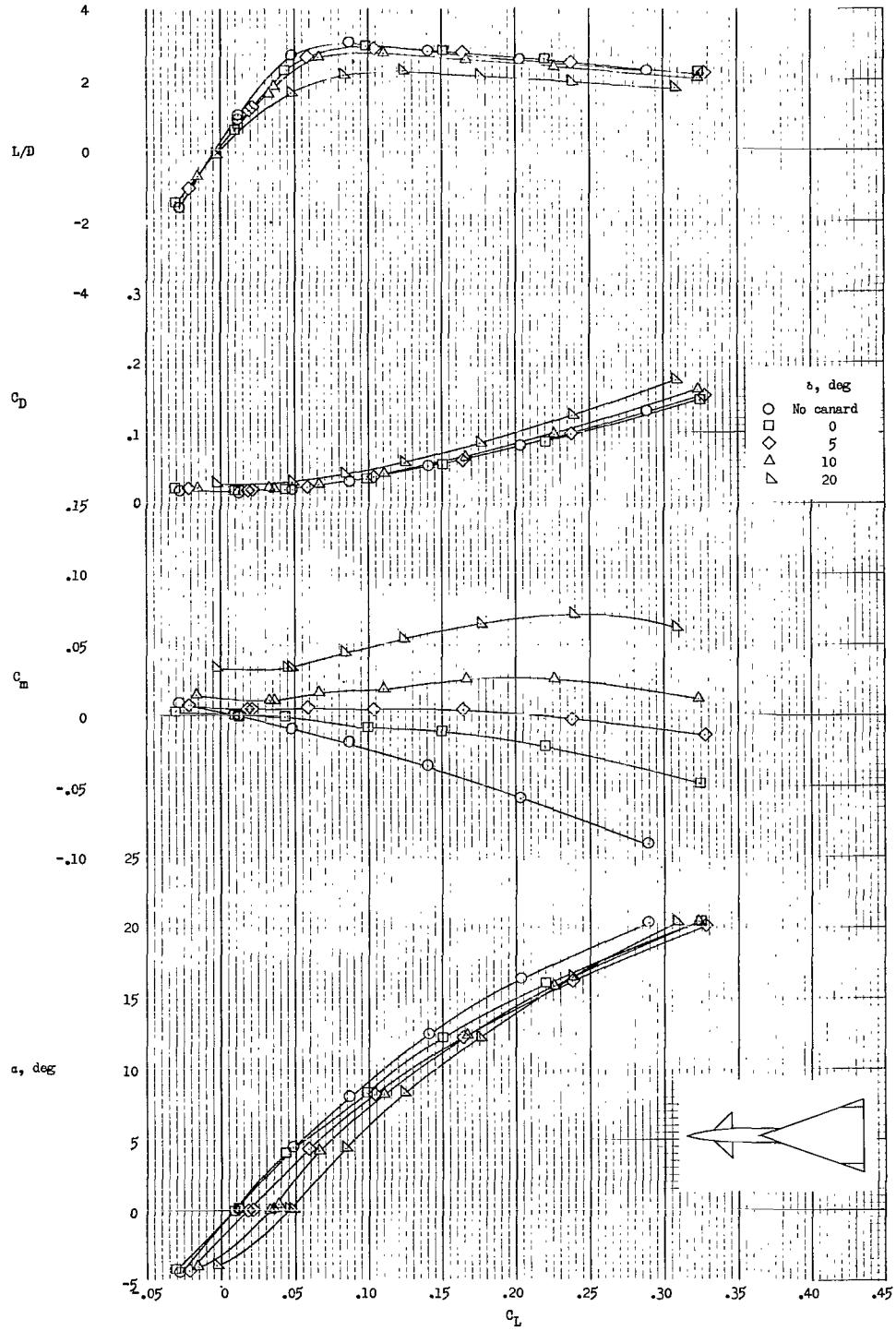

Figure 8.- Longitudinal aerodynamic characteristics of configuration $W_1B_2C_1$ with canard off and with various canard deflections.

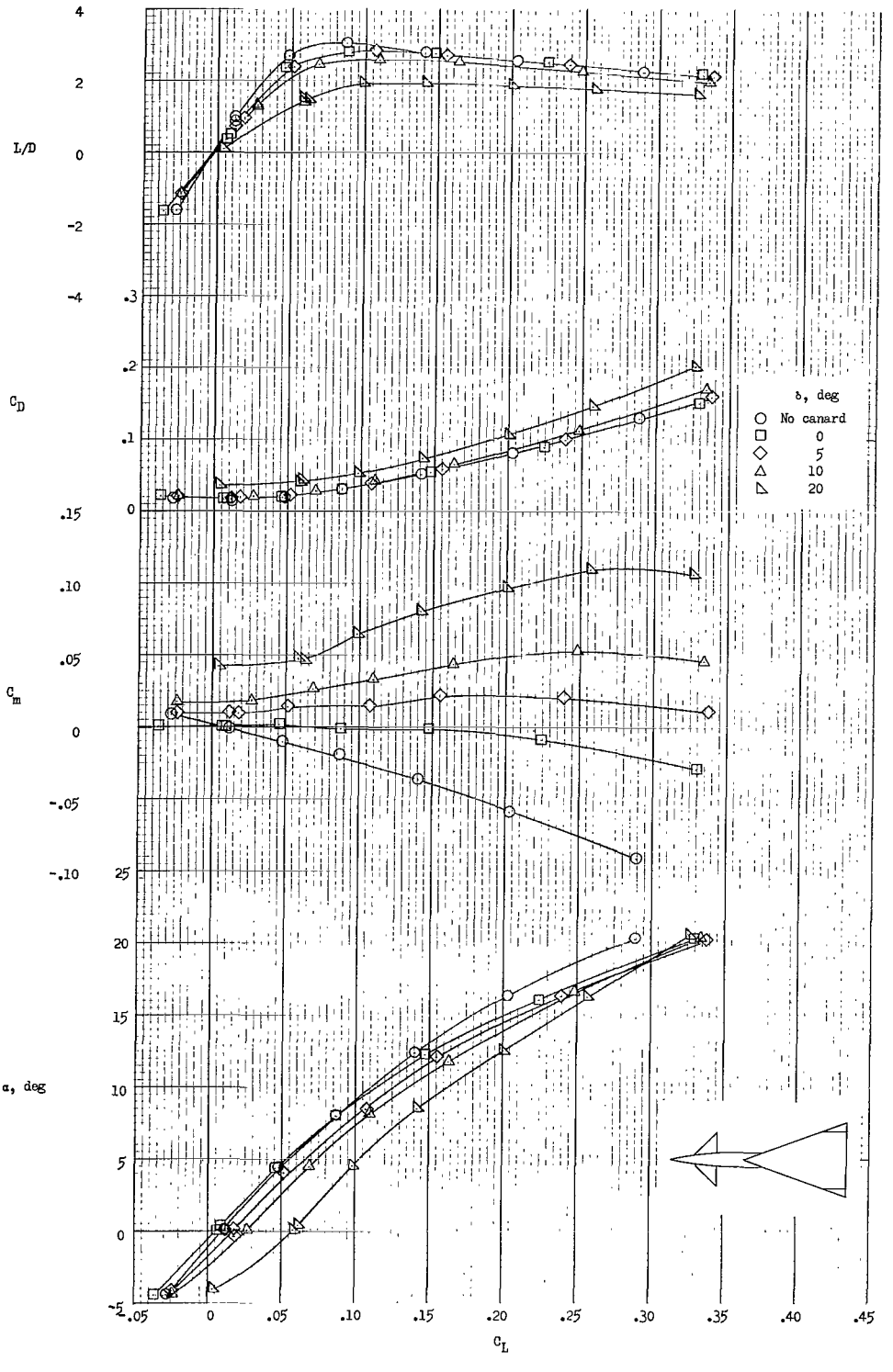

Figure 9.- Longitudinal aerodynamic characteristics of configuration $W_1B_2C_2$ with canard off and with various canard deflections.

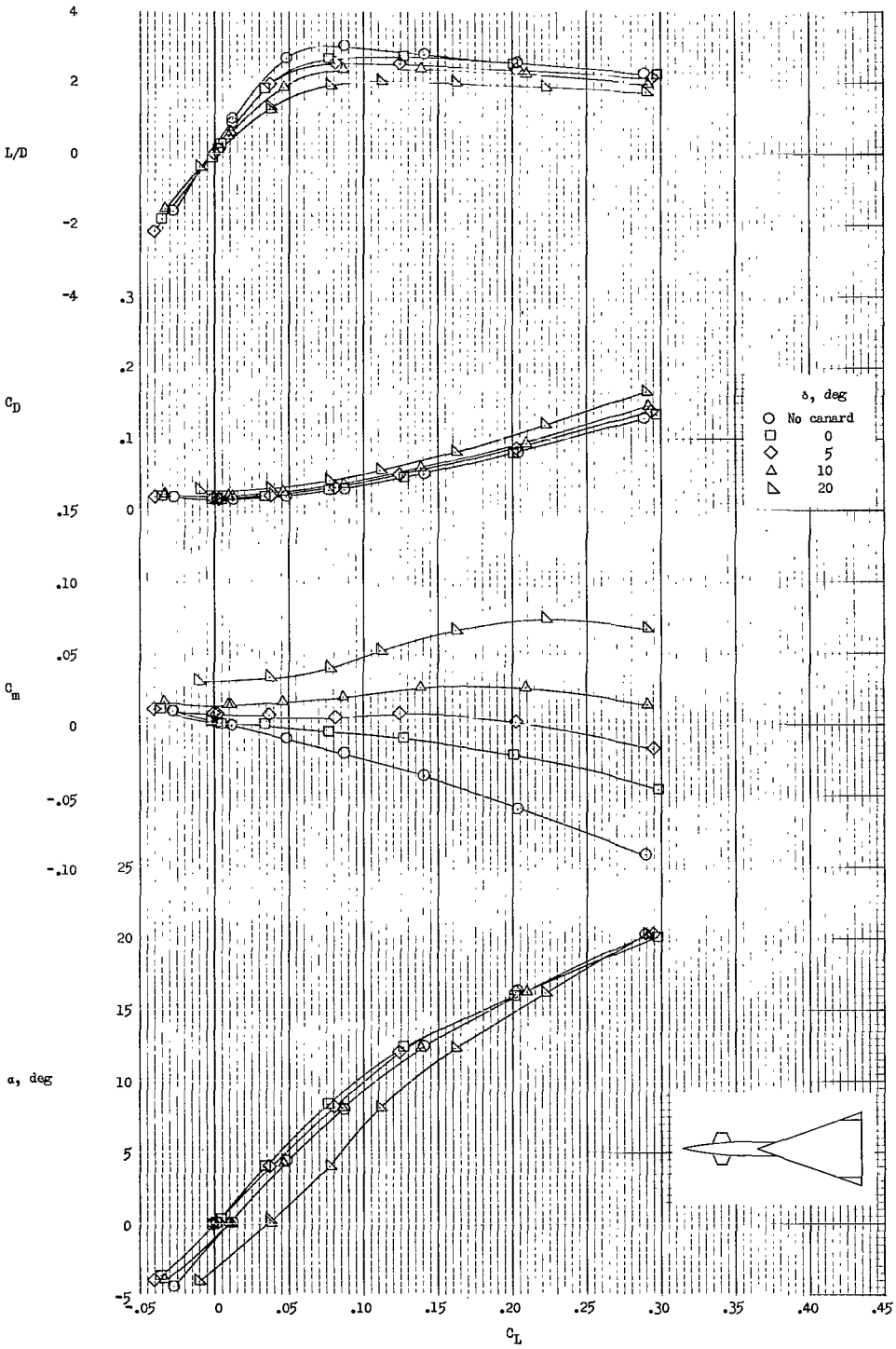

Figure 10.- Longitudinal aerodynamic characteristics of configuration $W_1B_2C_3$ with canard off and with various canard deflections.

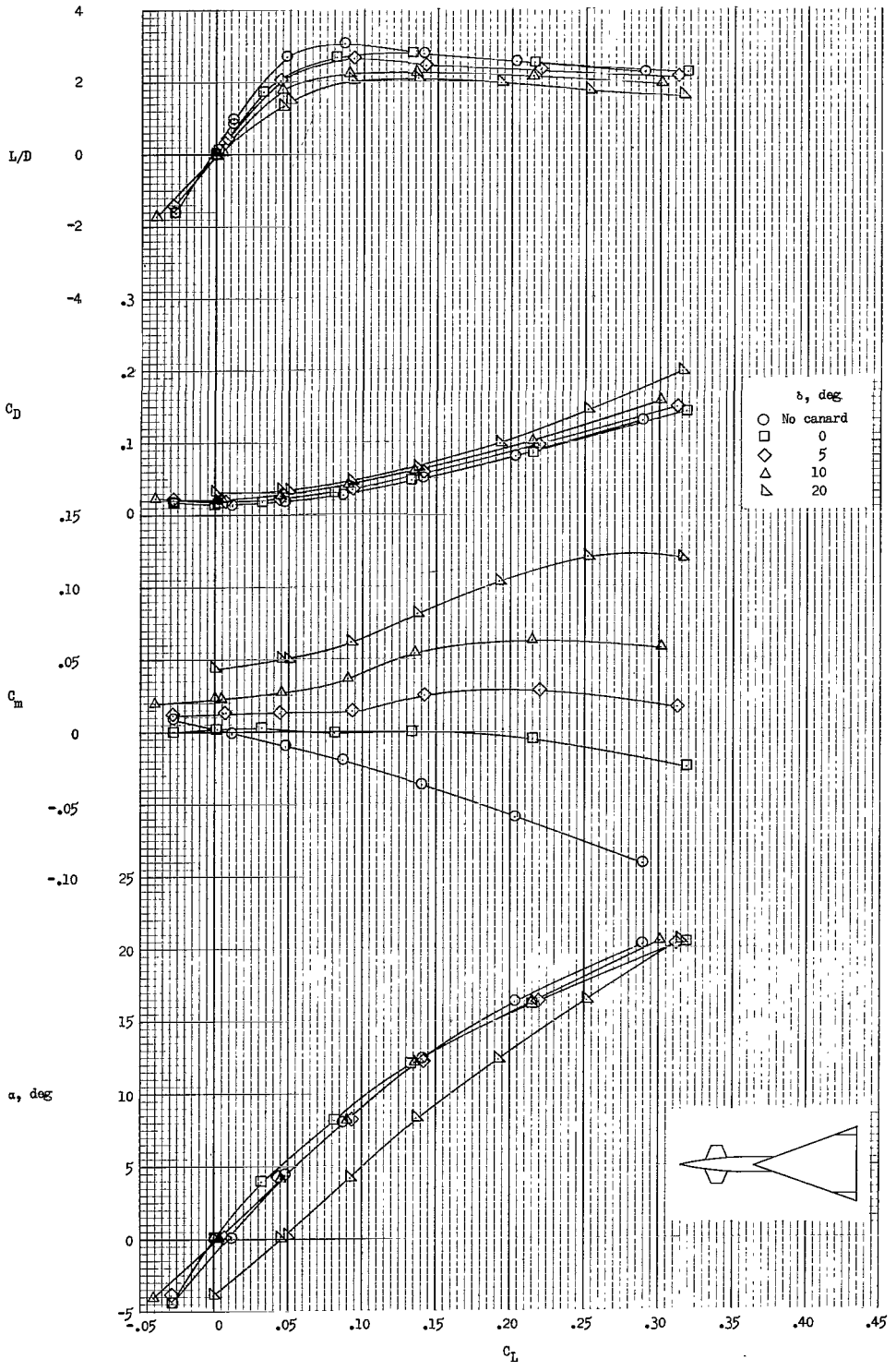

Figure 11.- Longitudinal aerodynamic characteristics of configuration $W_1B_2C_4$ with canard off and with various canard deflections.

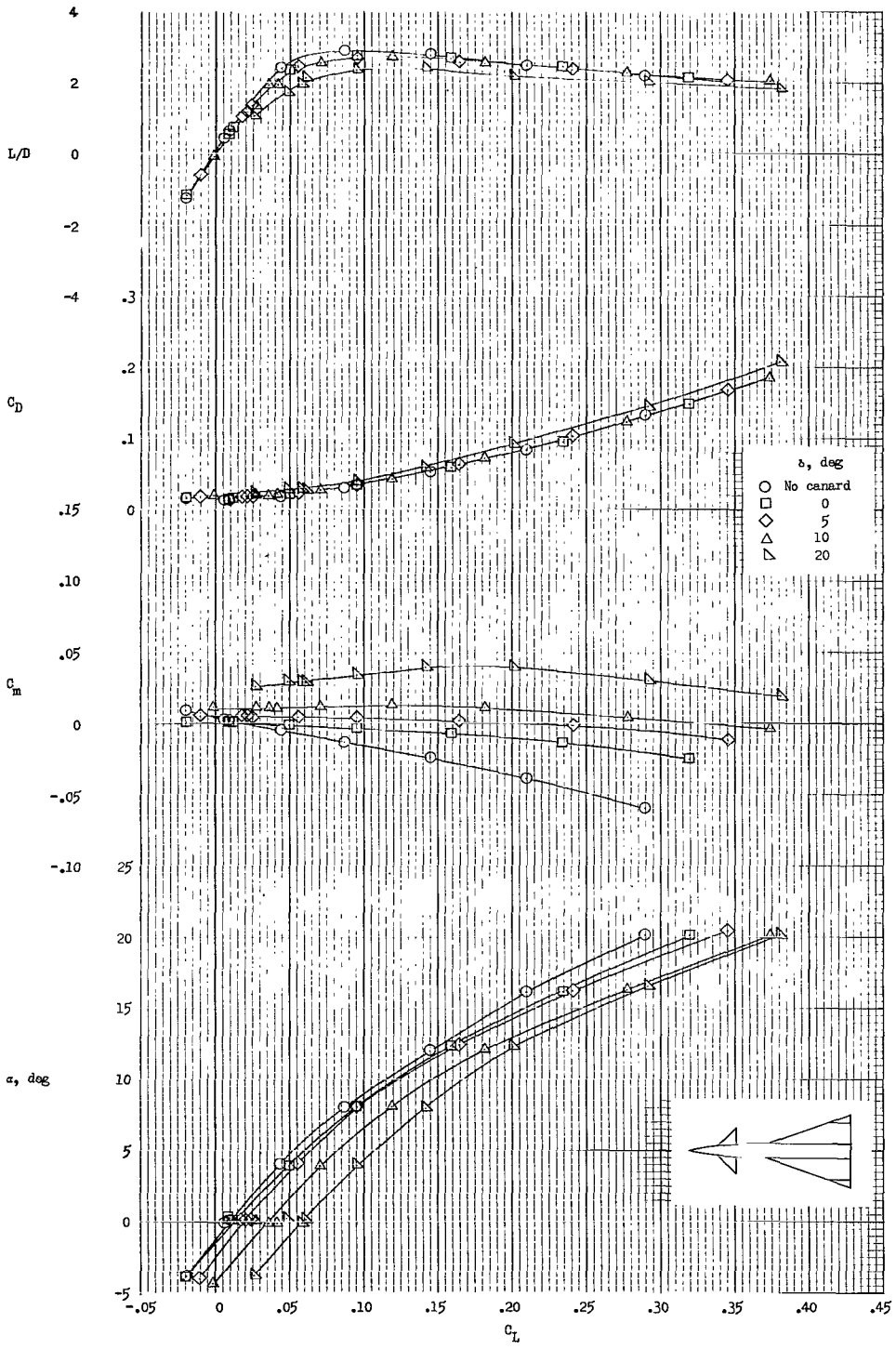

Figure 12.- Longitudinal aerodynamic characteristics of configuration $W_2B_1C_1$ with canard off and with various canard deflections.

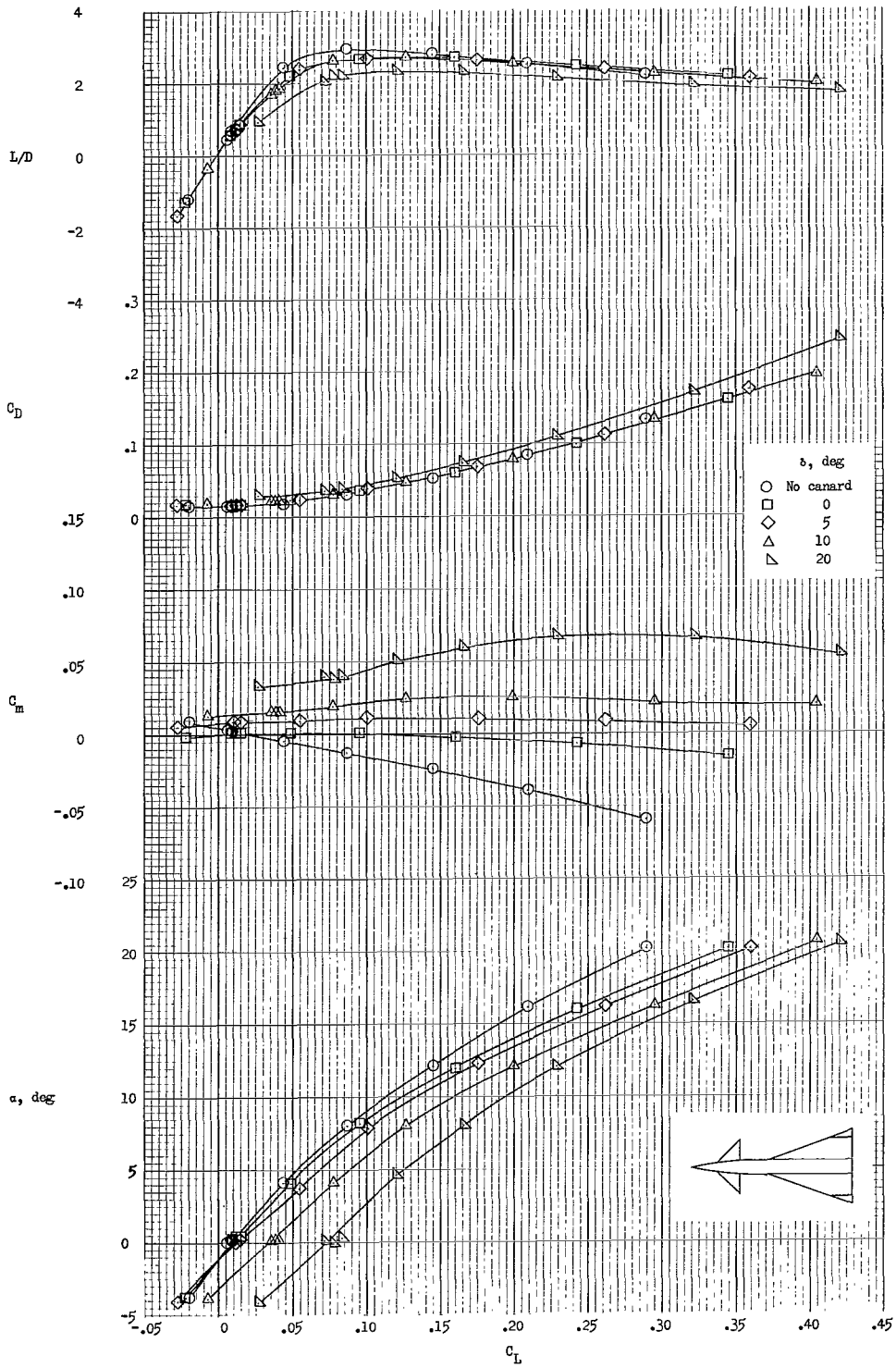

Figure 13.- Longitudinal aerodynamic characteristics of configuration $W_2B_1C_2$ with canard off and with various canard deflections.

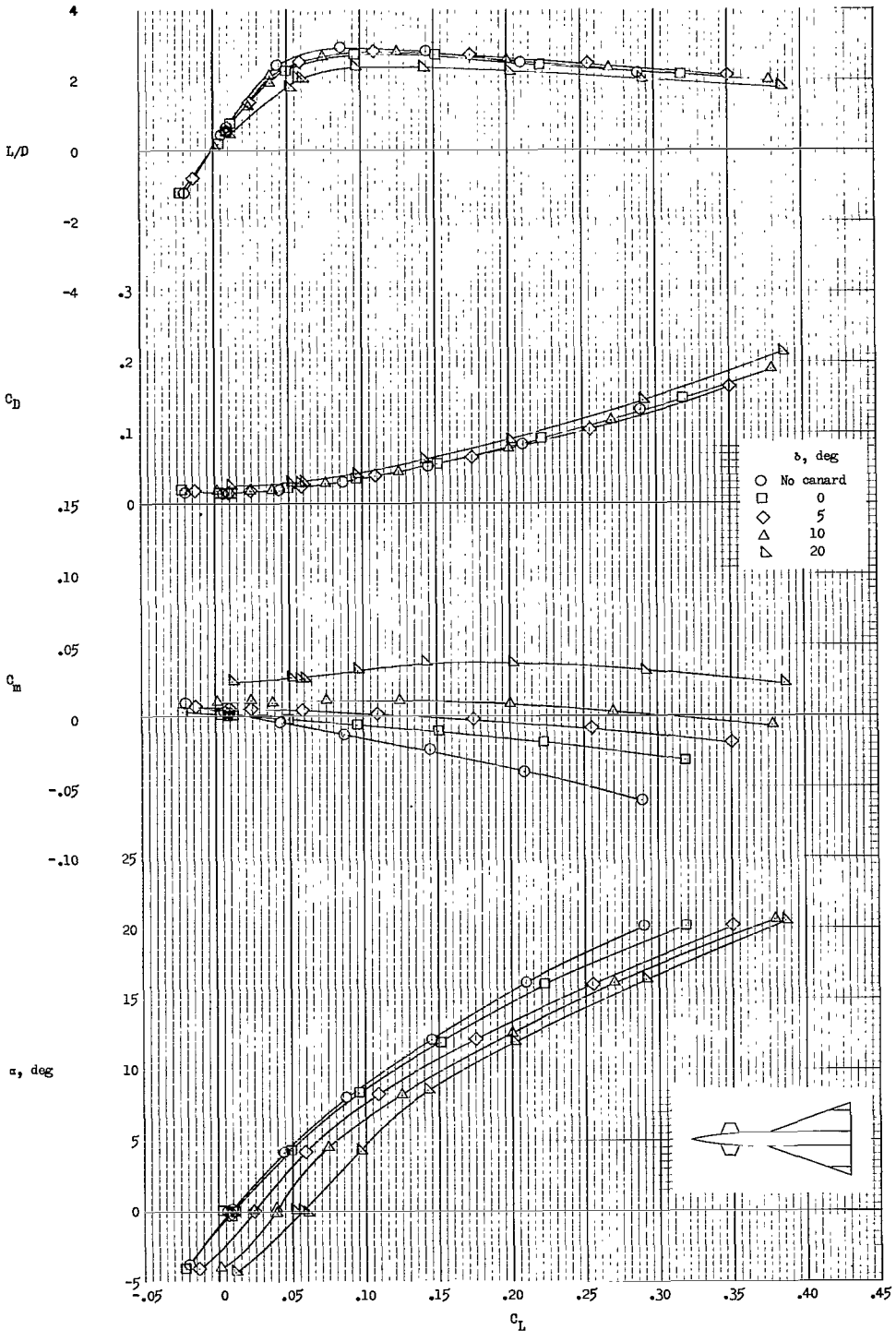

Figure 14.- Longitudinal aerodynamic characteristics of configuration $W_2B_1C_3$ with canard off and with various canard deflections.

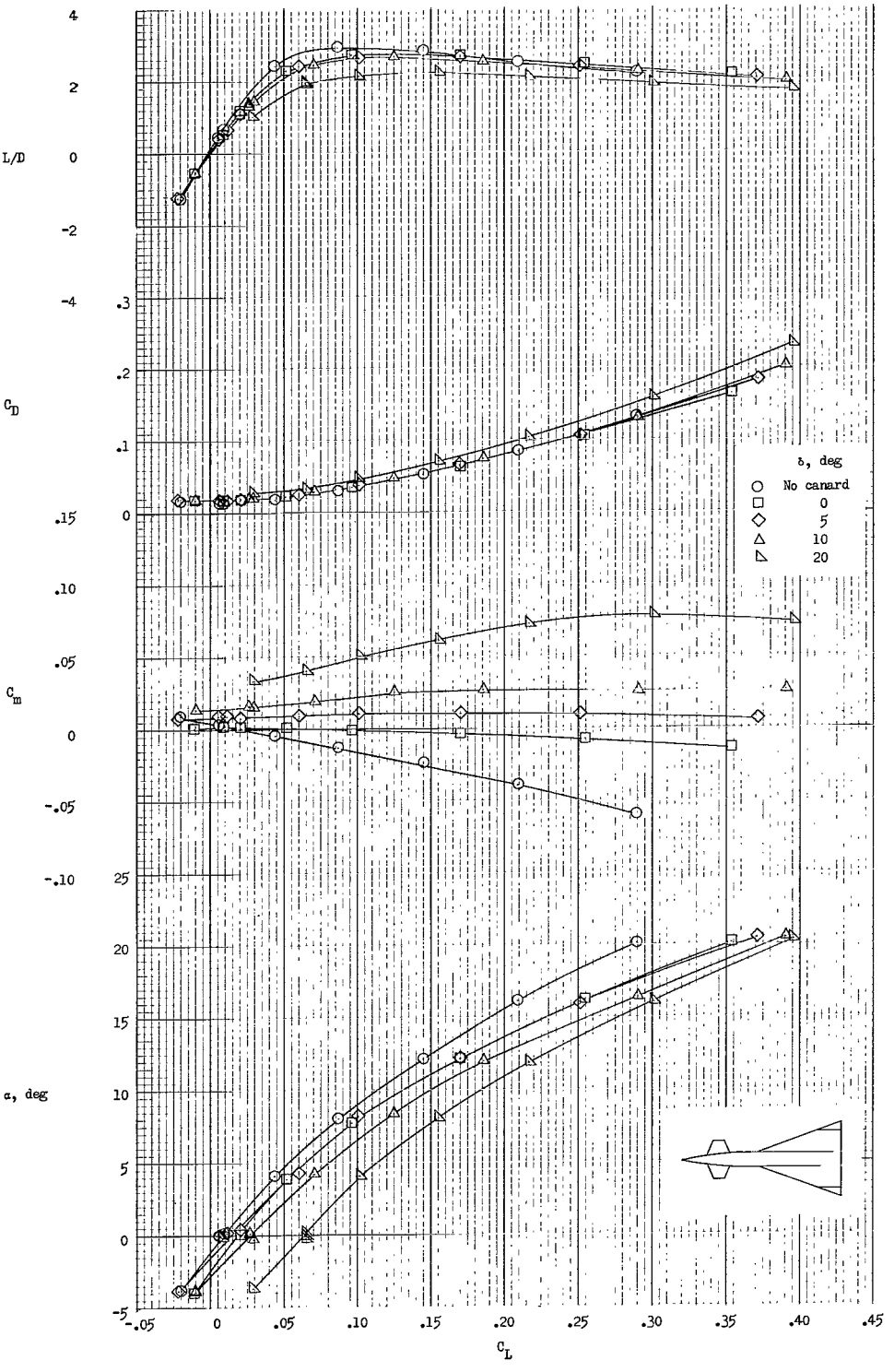

Figure 15.- Longitudinal aerodynamic characteristics of configuration $W_2B_1C_4$ with canard off and with various canard deflections.

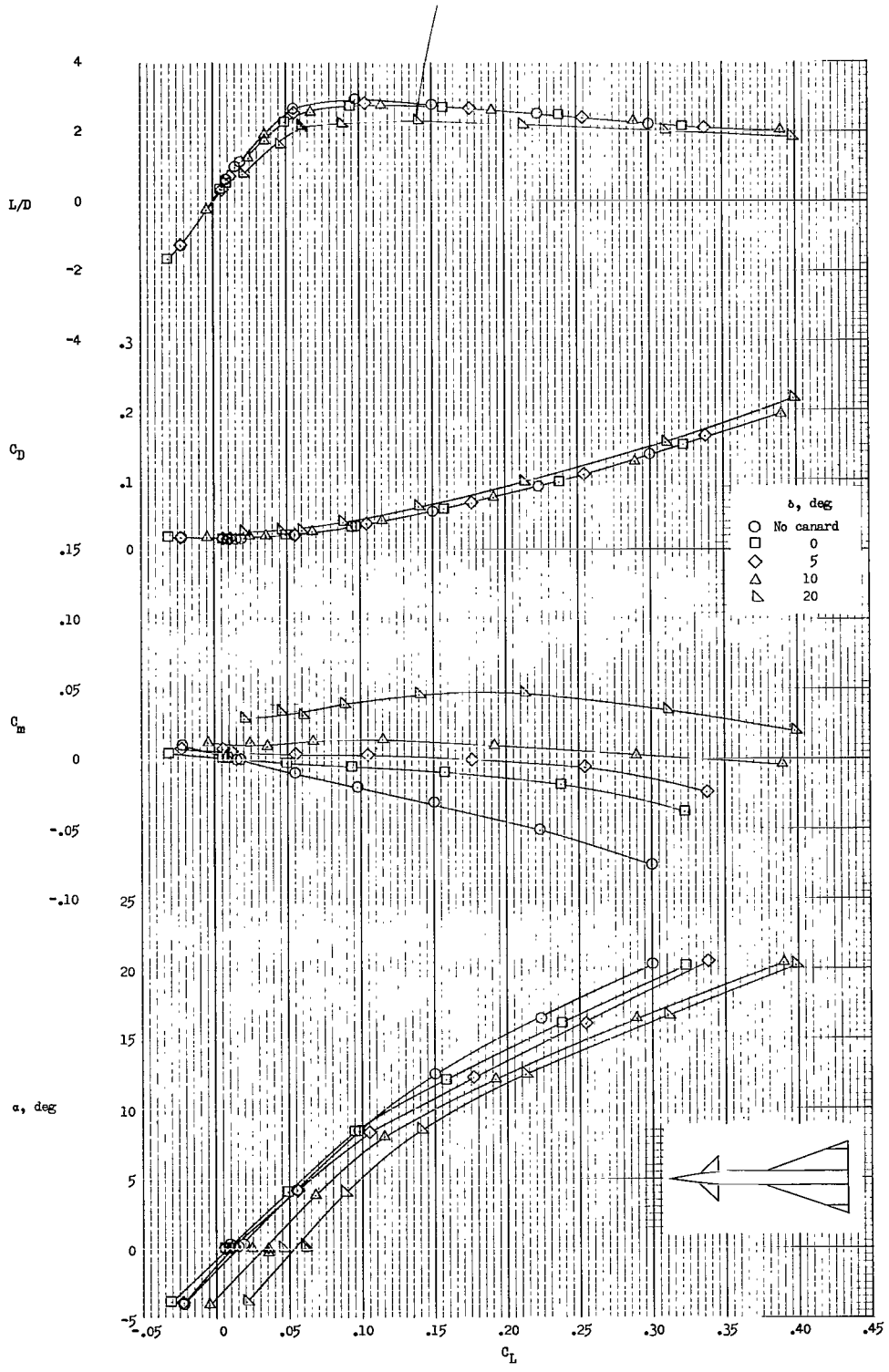

Figure 16.- Longitudinal aerodynamic characteristics of configuration $W_2B_2C_1$ with canard off and with various canard deflections.

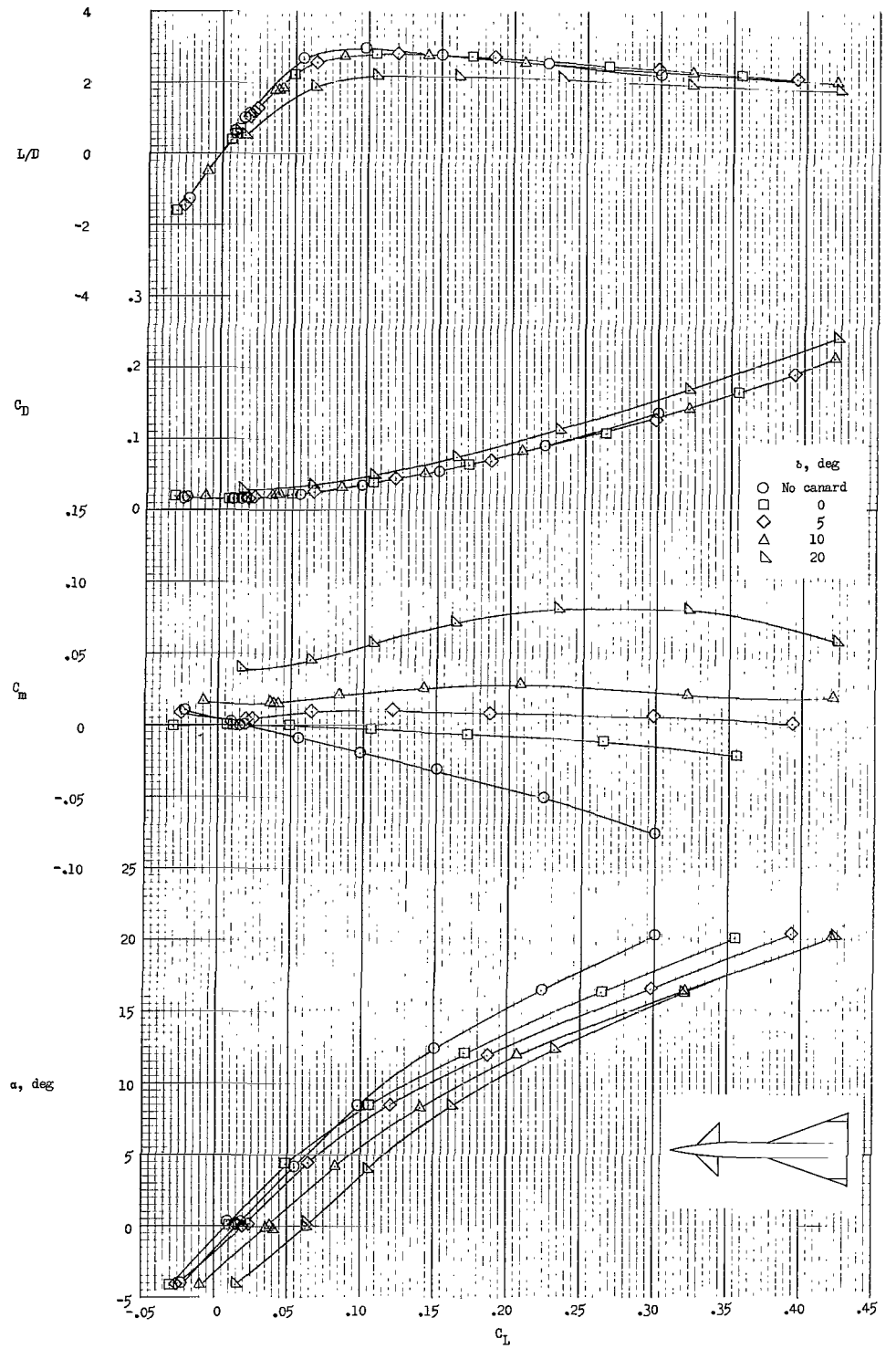

Figure 17.- Longitudinal aerodynamic characteristics of configuration $W_2B_2C_2$ with canard off and with various canard deflections.

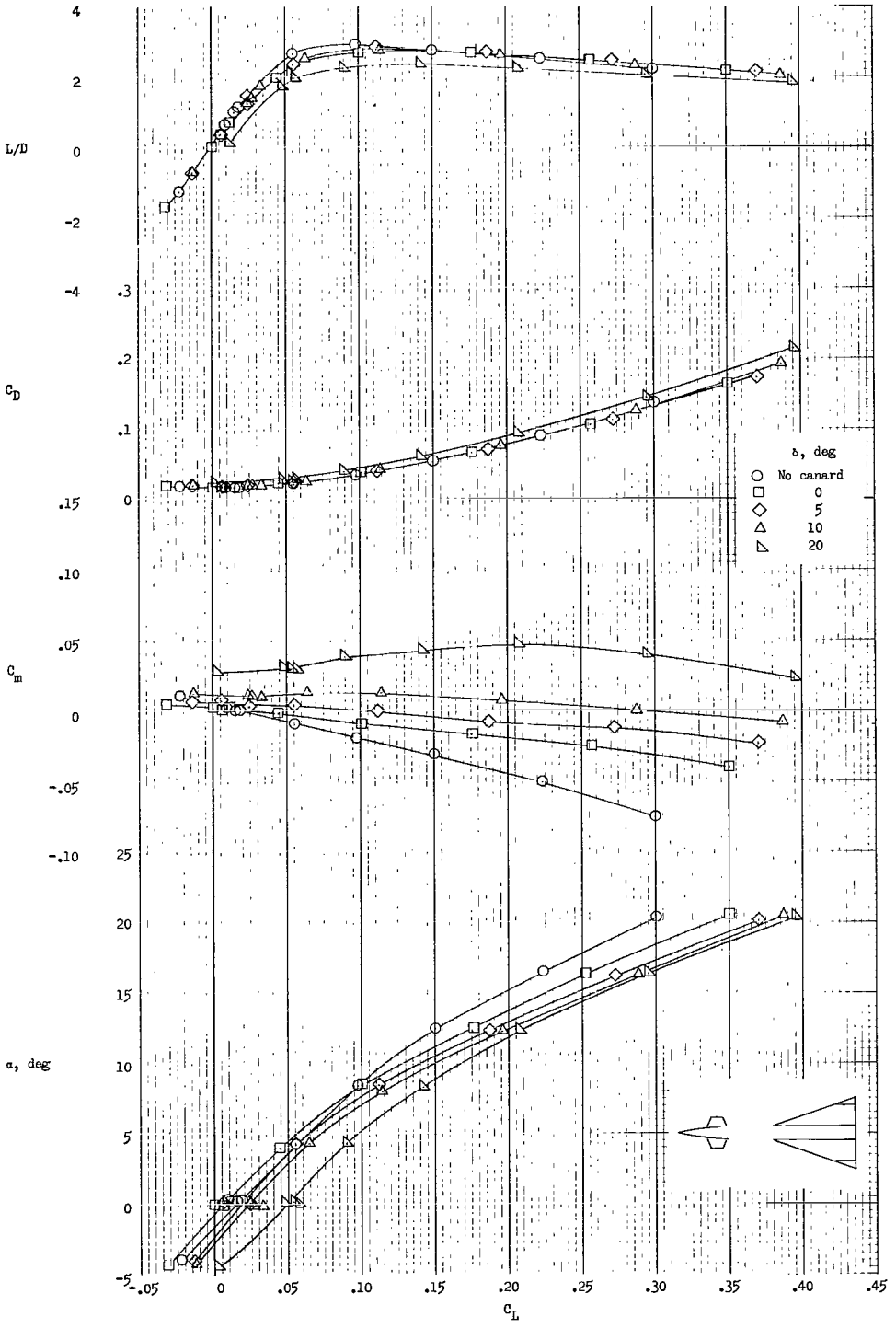

Figure 18.- Longitudinal aerodynamic characteristics of configuration $W_2B_2C_3$ with canard off and with various canard deflections.

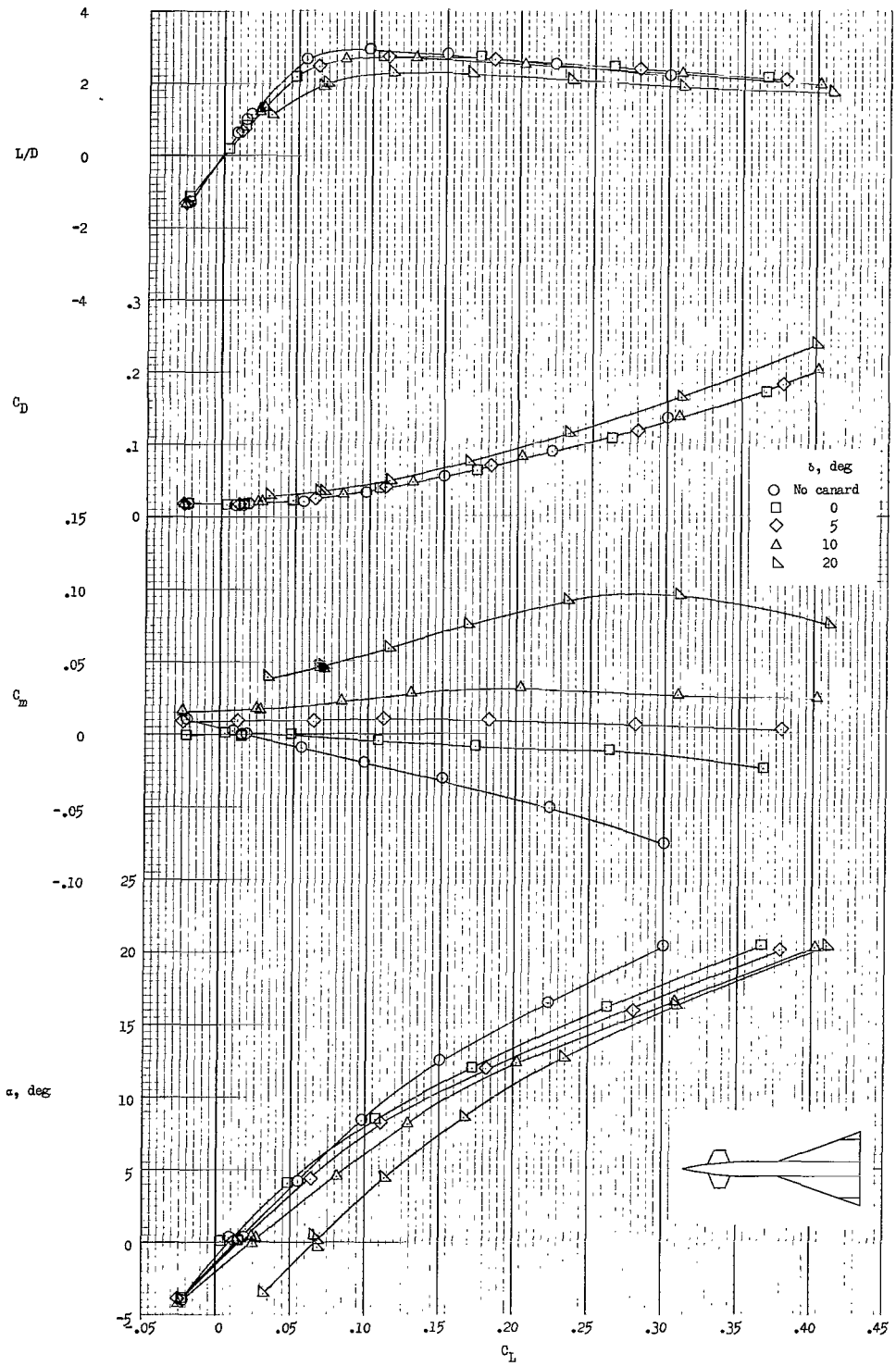

Figure 19.- Longitudinal aerodynamic characteristics of configuration $W_2B_2C_4$ with canard off and with various canard deflections.

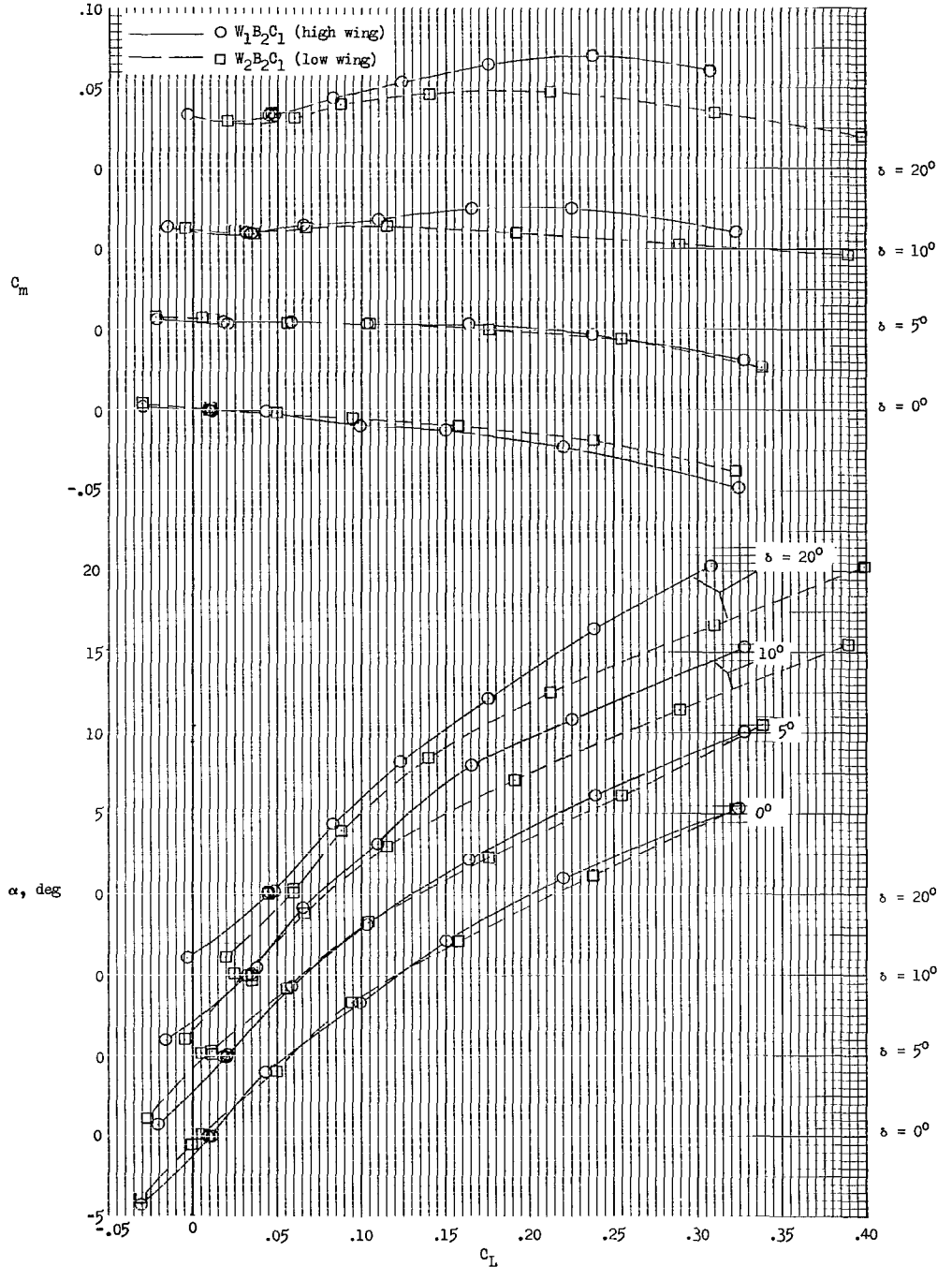

(a) Long-body small-delta-canard configurations.

Figure 20.- Effect of wing position.

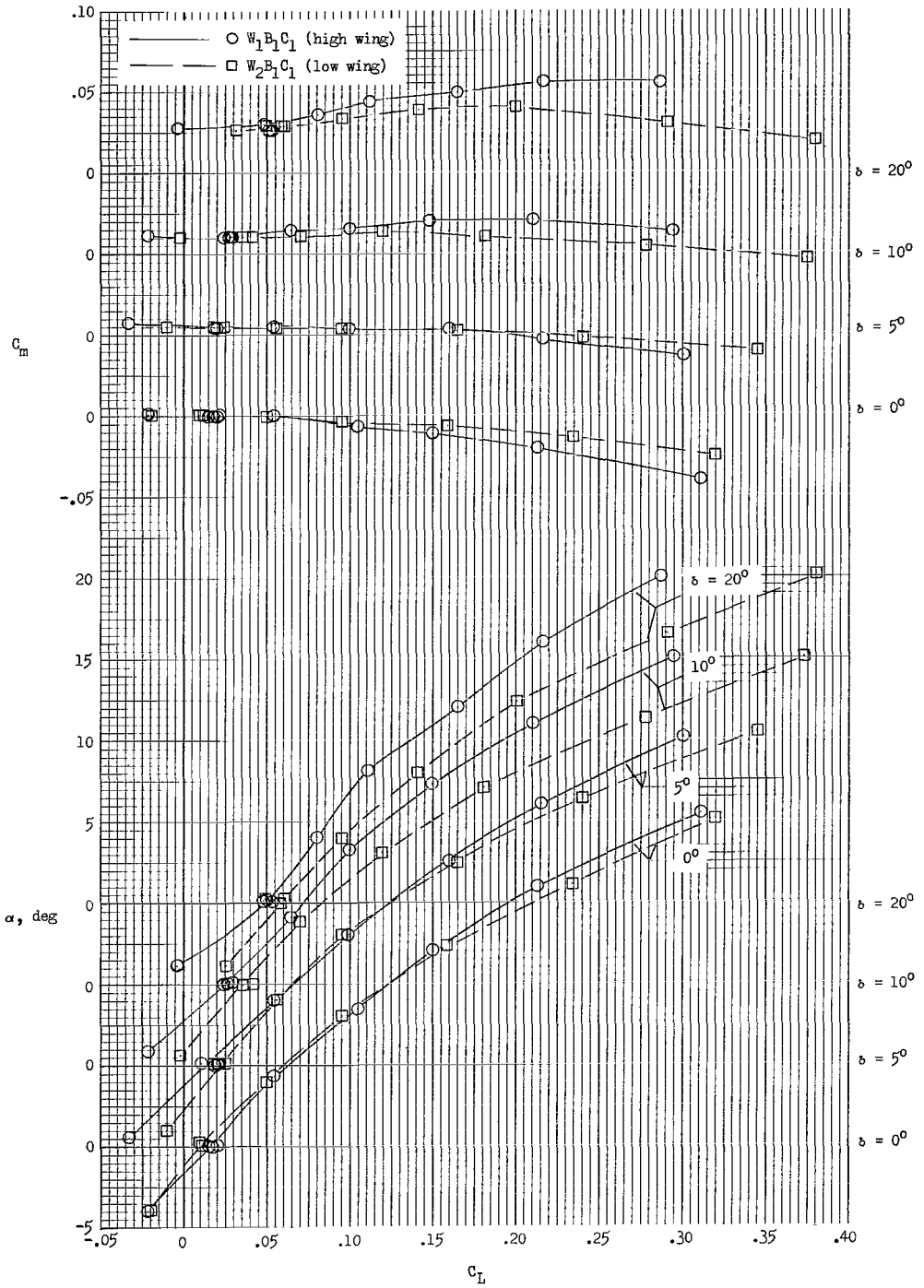

(b) Short-body small-delta-canard configurations.

Figure 20.- Continued.

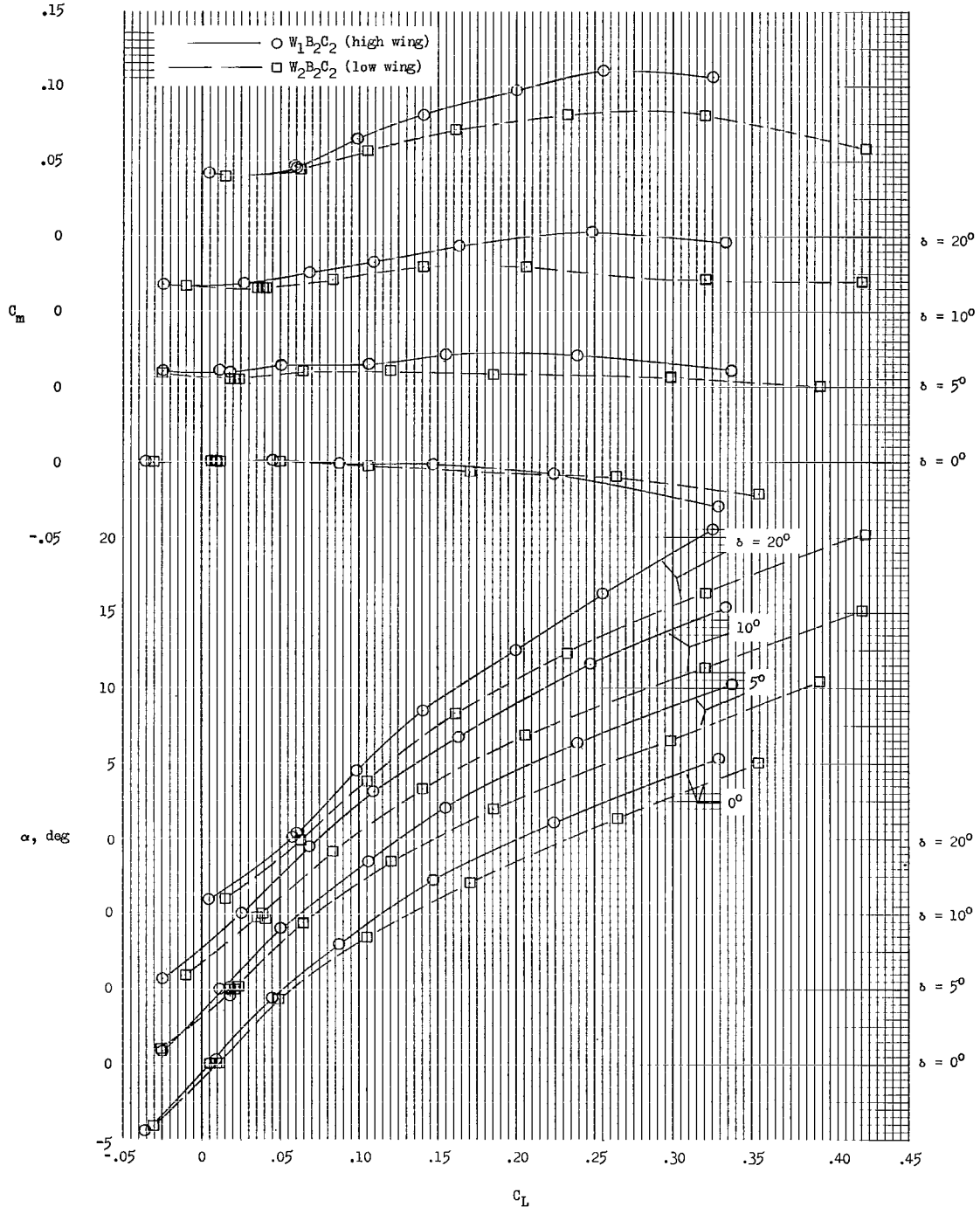

(c) Long-body large-delta-canard configurations.

Figure 20.- Continued.

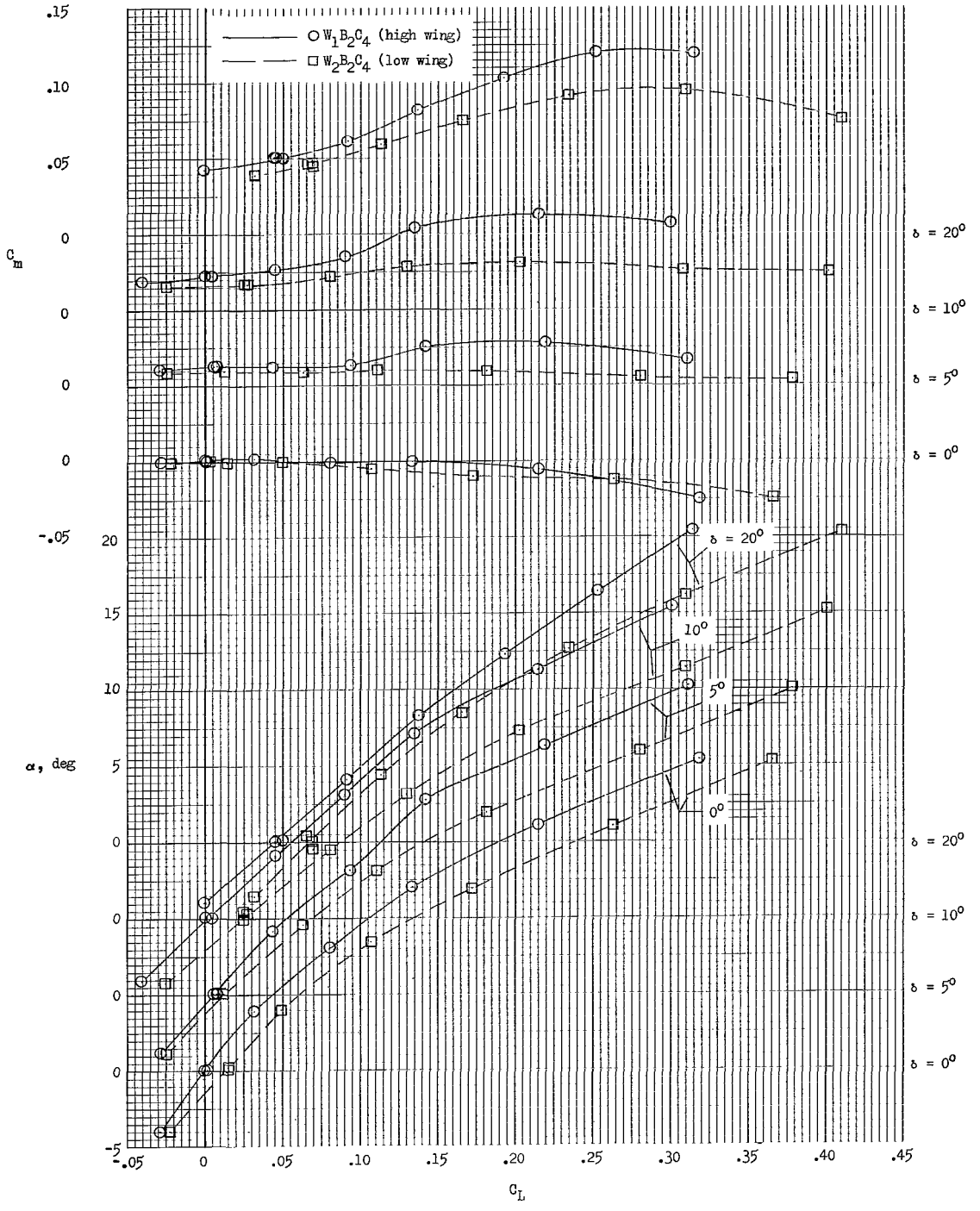

(d) Long-body large-trapezoidal canard configurations.

Figure 20.- Concluded.

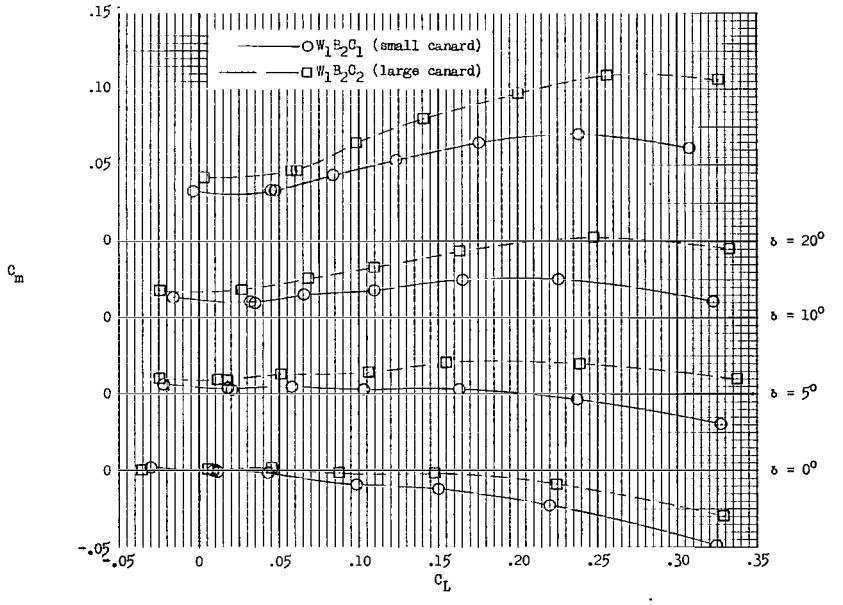

(a) Common moment reference center location at 60 percent of total body length.

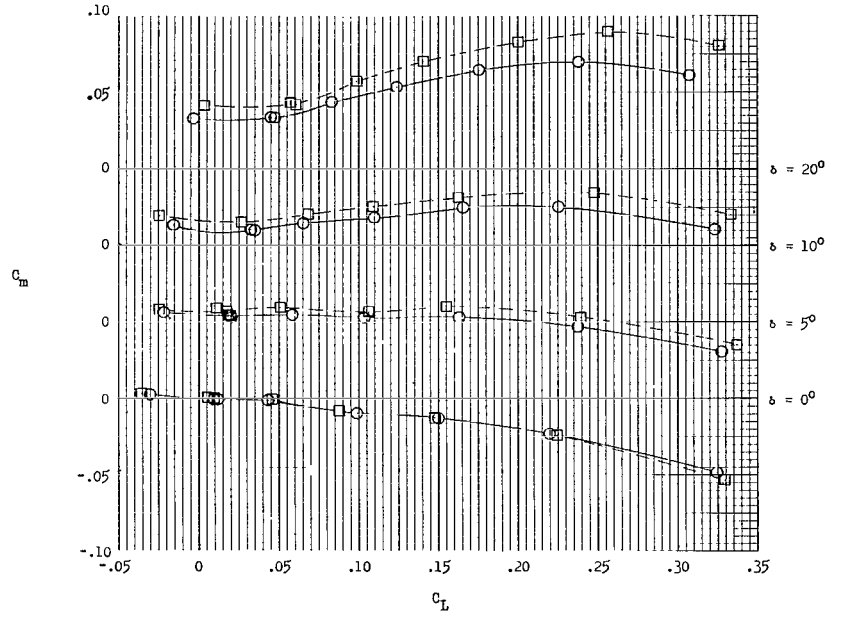

(b) Common static margin at $C_L = 0$ and $\delta = 0$. $\left(\frac{\partial C_m}{\partial C_L}\right)_{\substack{C_L=0 \\ \delta=0}} = -0.051$.

Figure 21.- Effect of canard size on the high-wing long-body delta-canard configuration. Moment reference center for configuration $W_1B_2C_2$ (large canard) at 57.5 percent of total body length.

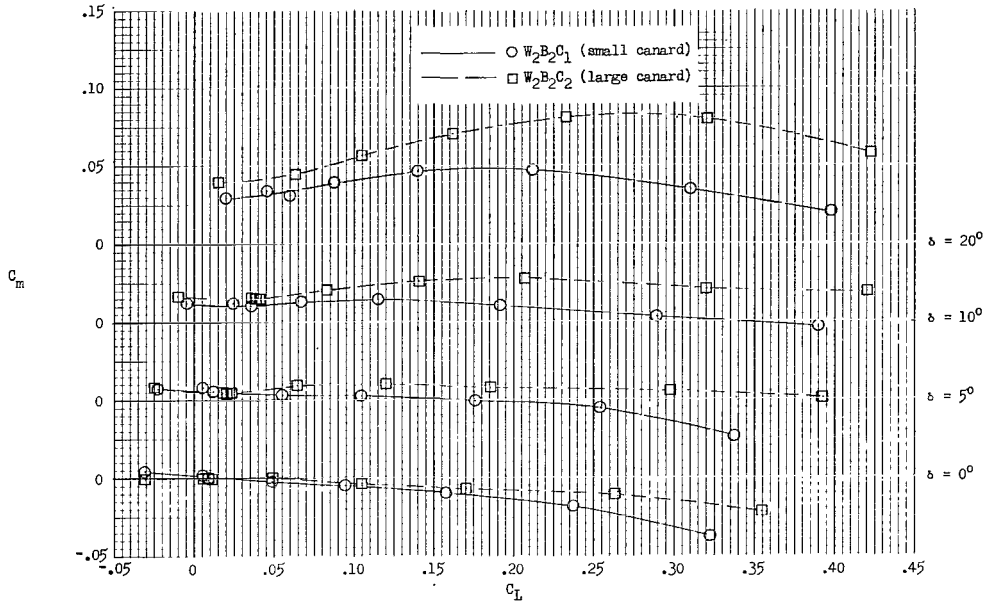

(a) Common moment reference center location at 60 percent of total body length.

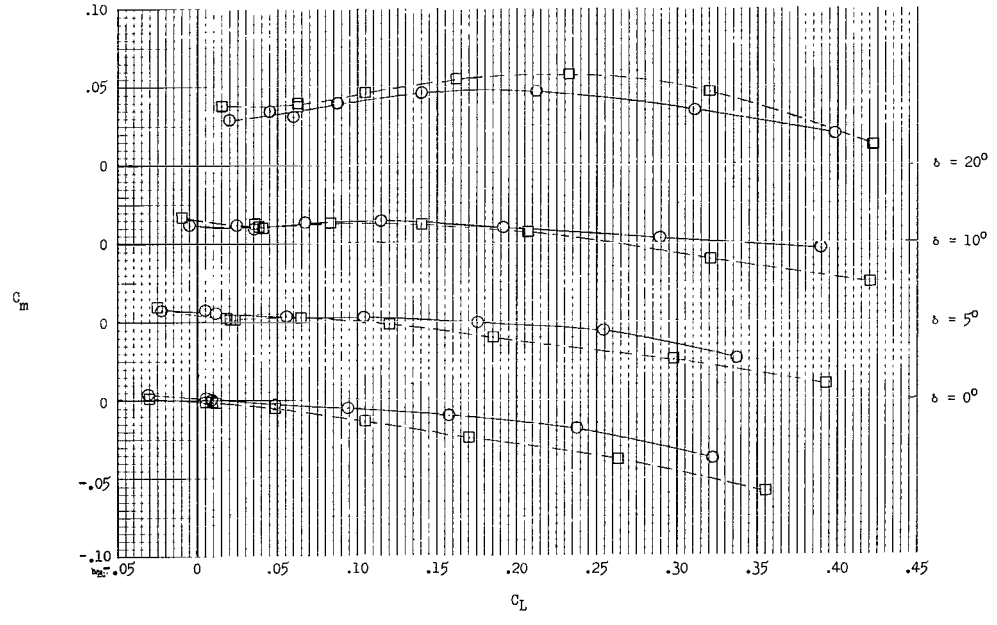

(b) Common static margin at $C_L = 0$ and $\delta = 0$. $\left(\frac{\partial C_m}{\partial C_L}\right)_{\substack{C_L=0 \\ \delta=0}} = -0.090$.

Figure 22.- Effect of canard size on the low-wing long-body delta-canard configuration. Moment reference center for configuration $W_2B_2C_2$ at 53.6 percent of total body length.

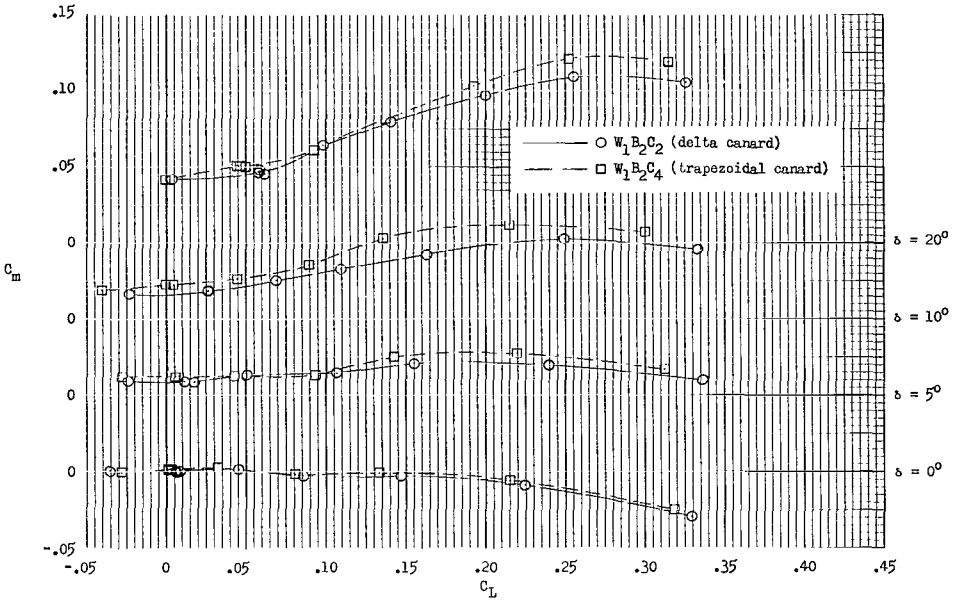

(a) High-wing long-body large-canard configuration.

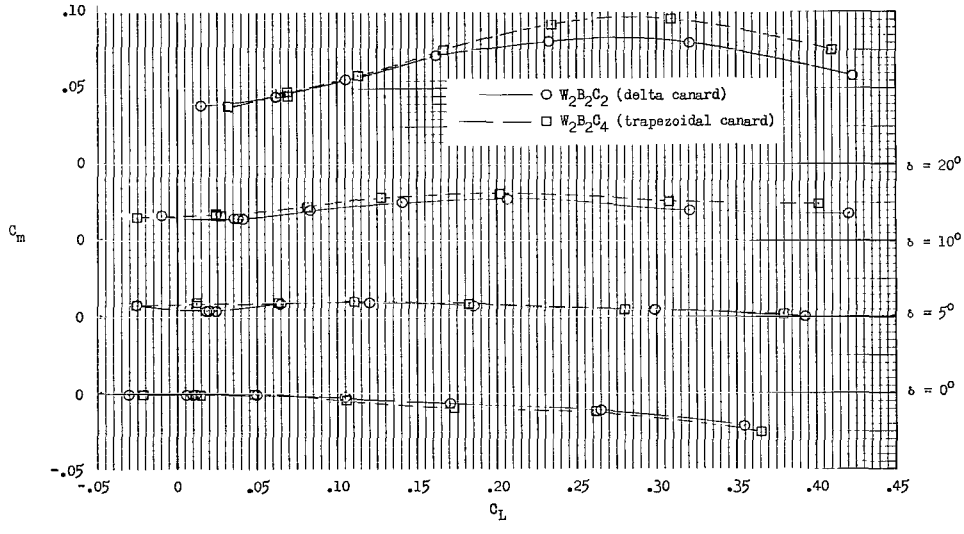

(b) Low-wing long-body large-canard configuration.

Figure 23.- Effect of canard planform shape.

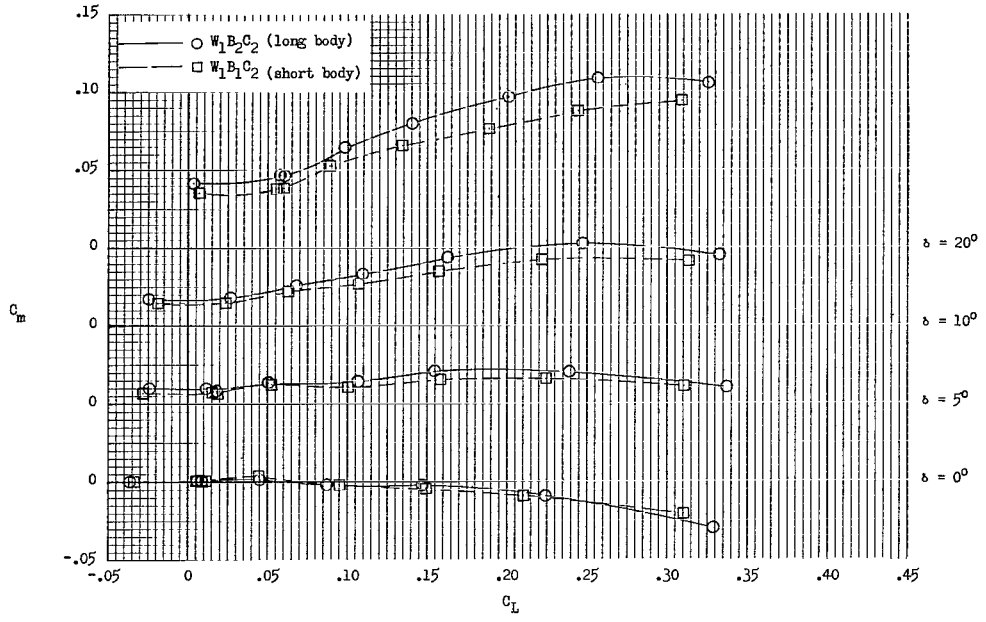

(a) High-wing large-delta-canard configuration.

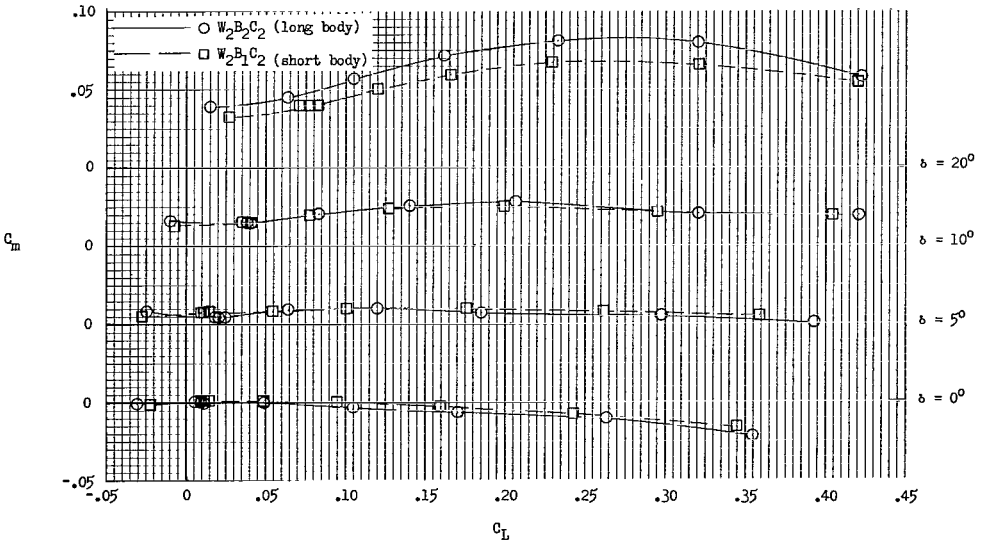

(b) Low-wing large-delta-canard configuration.

Figure 24.- Effect of body length.

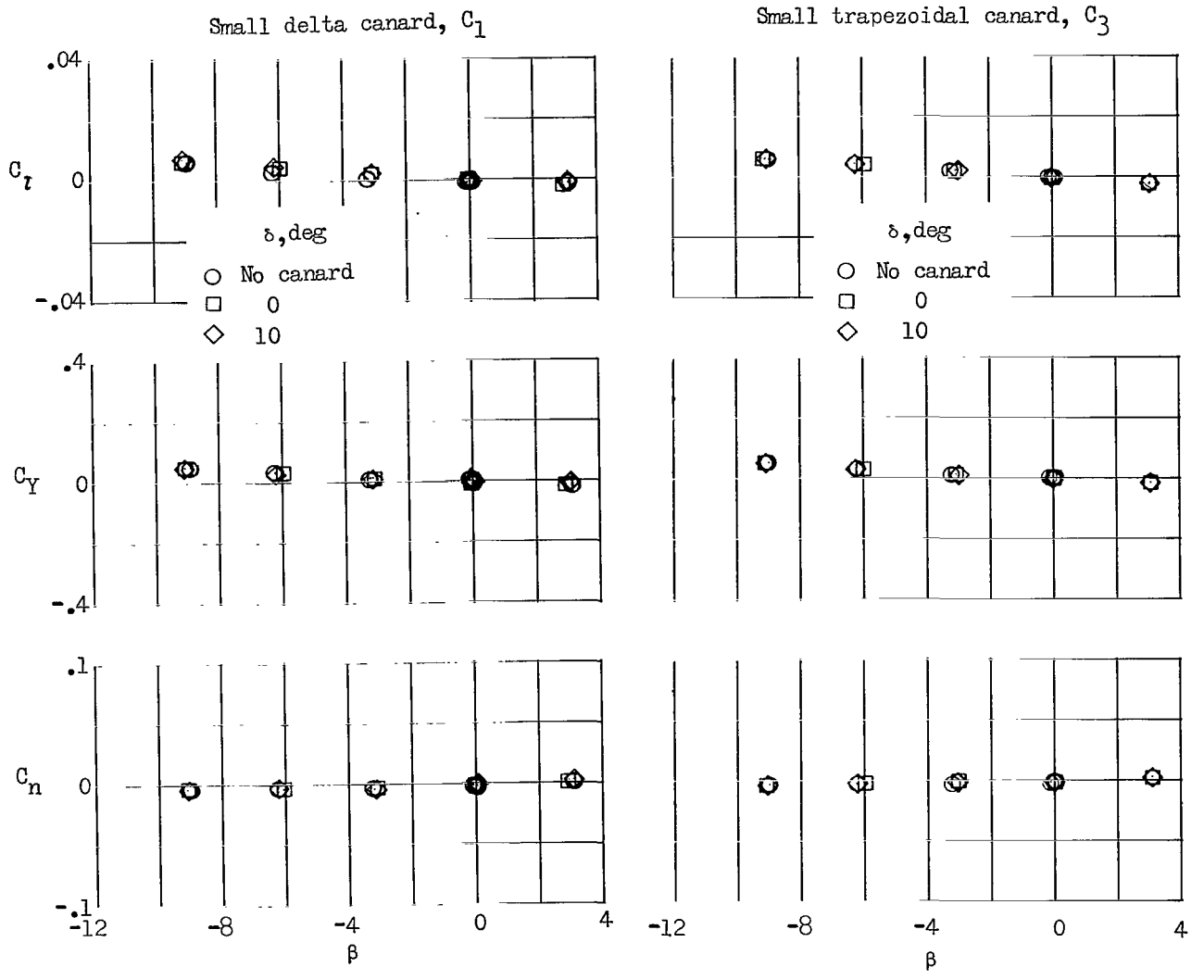

Figure 25.- Effect of canard deflection on directional and lateral aerodynamic characteristics of configuration W_1B_2C. $\alpha = 0$.

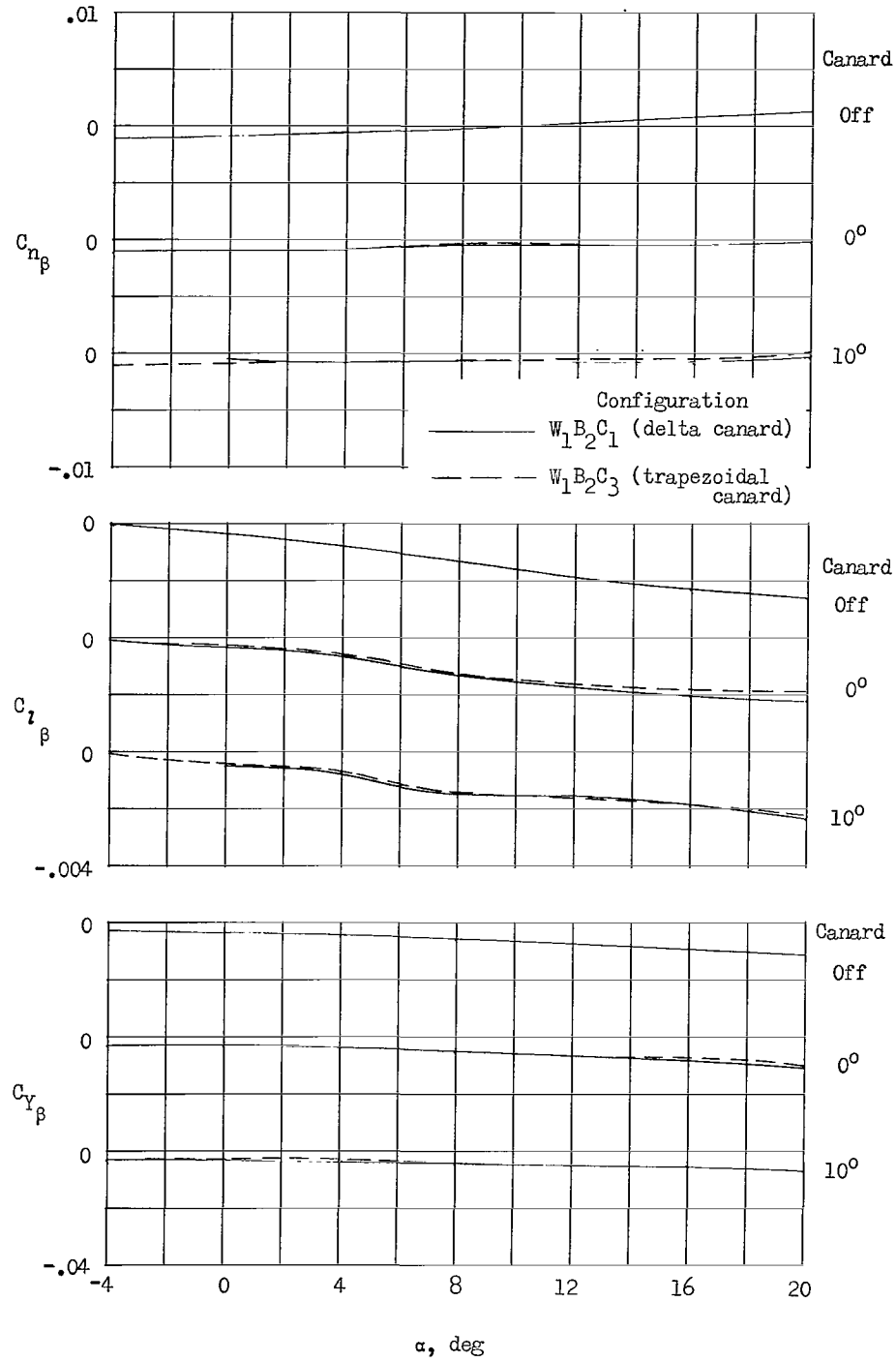

(a) Variation of lateral and directional stability derivatives with angle of attack. Vertical tails off.

Figure 26.- Effect of canard planform shape on the lateral and directional stability characteristics of configuration W_1B_2.

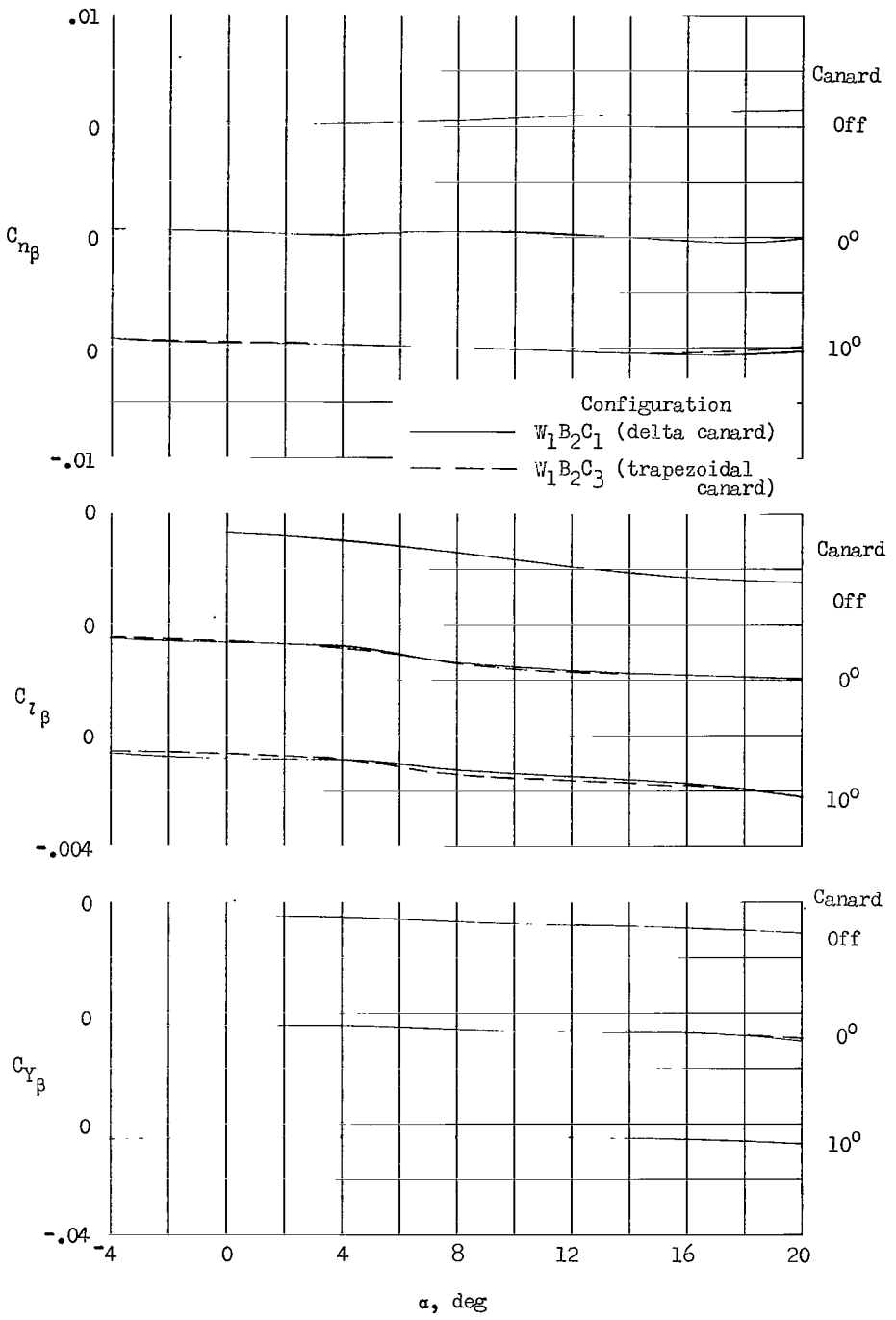

(b) Variation of lateral and directional stability derivatives with angle of attack. Vertical tails on.

Figure 26.- Concluded.

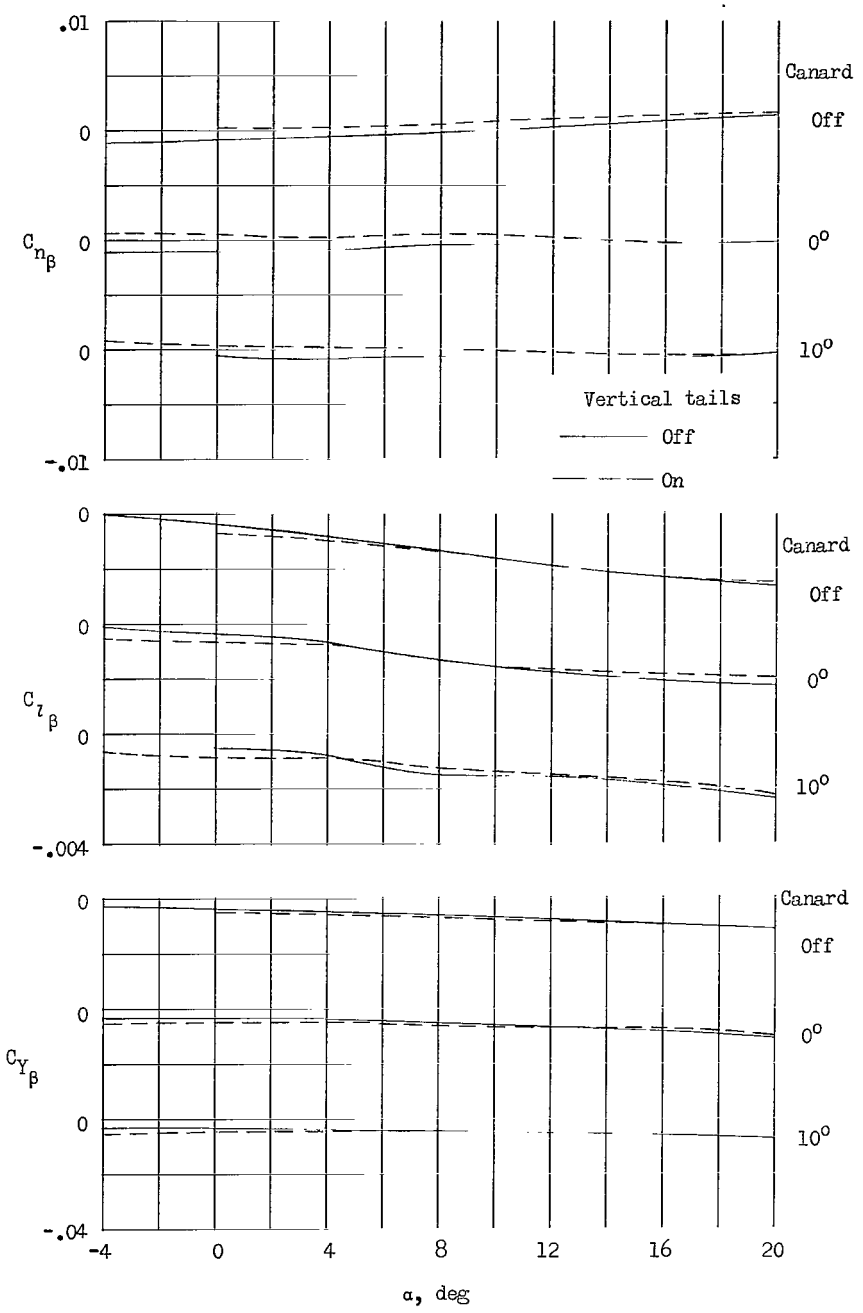

(a) Variation of stability derivatives with angle of attack. Configuration $W_1B_2C_1$.

Figure 27.- Effect of vertical tails on the directional and lateral aerodynamic characteristics of three configurations.

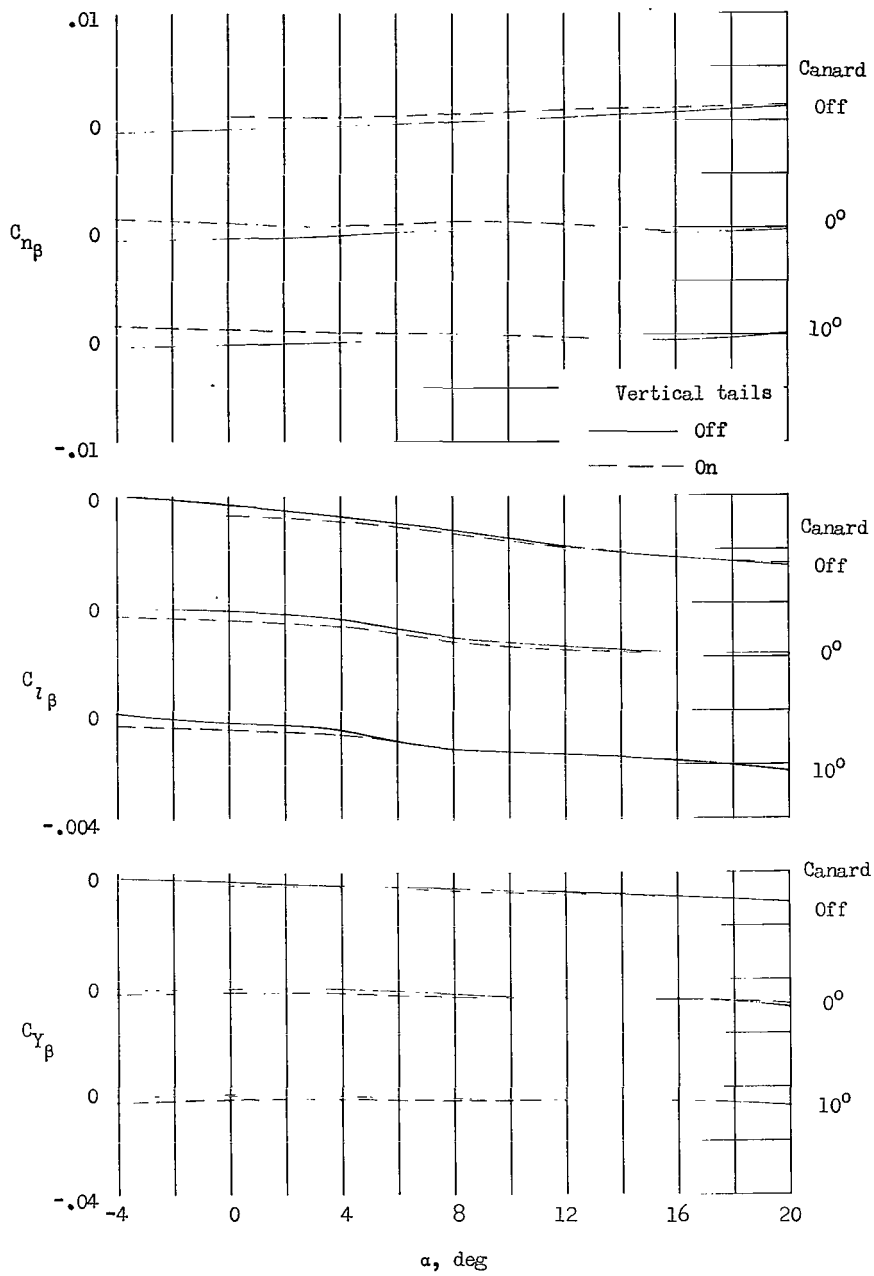

(b) Variation of stability derivatives with angle of attack. Configuration $W_1B_2C_3$.

Figure 27.- Continued.

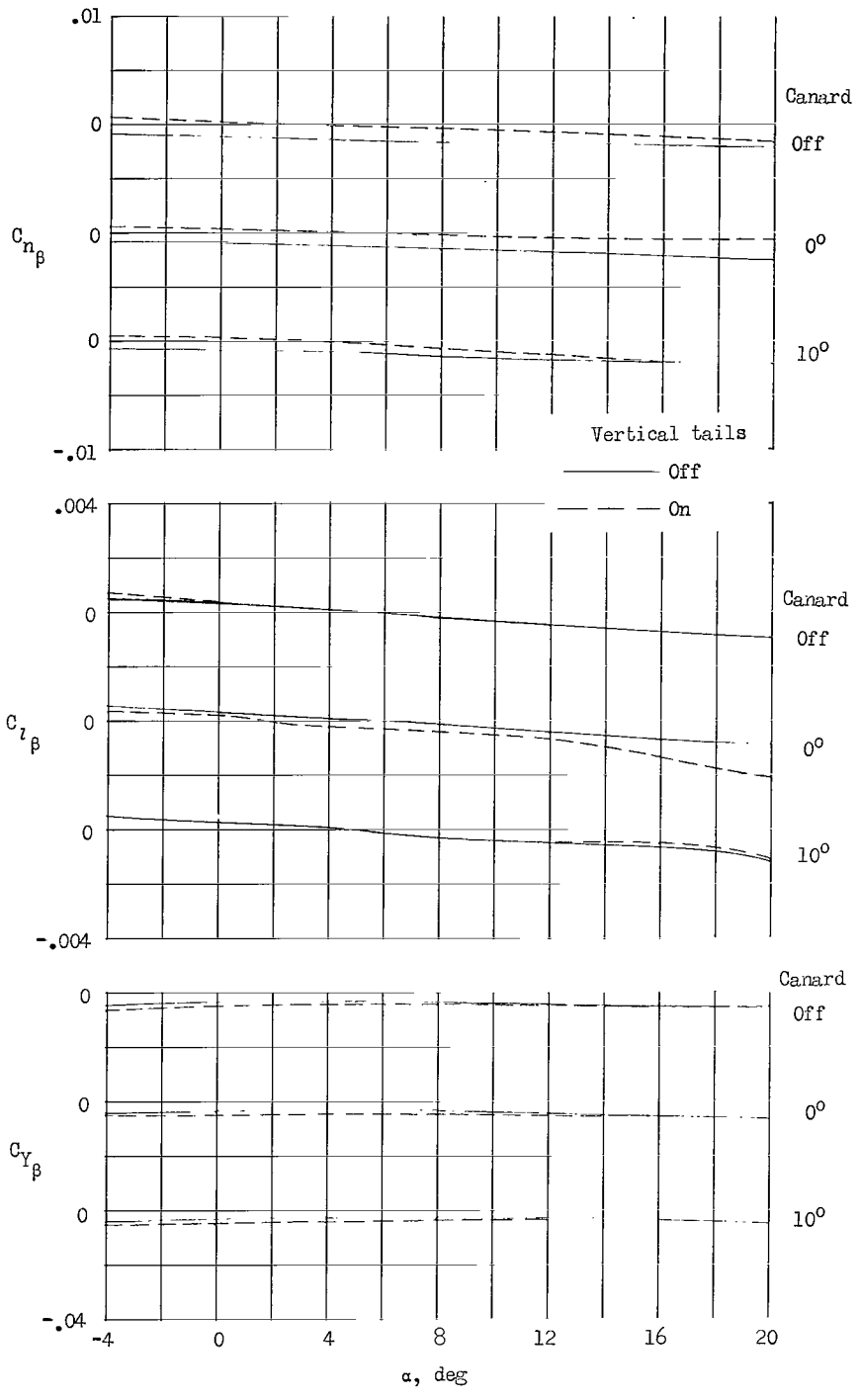

(c) Variation of stability derivatives with angle of attack. Configuration $W_2B_2C_1$.

Figure 27.- Concluded.

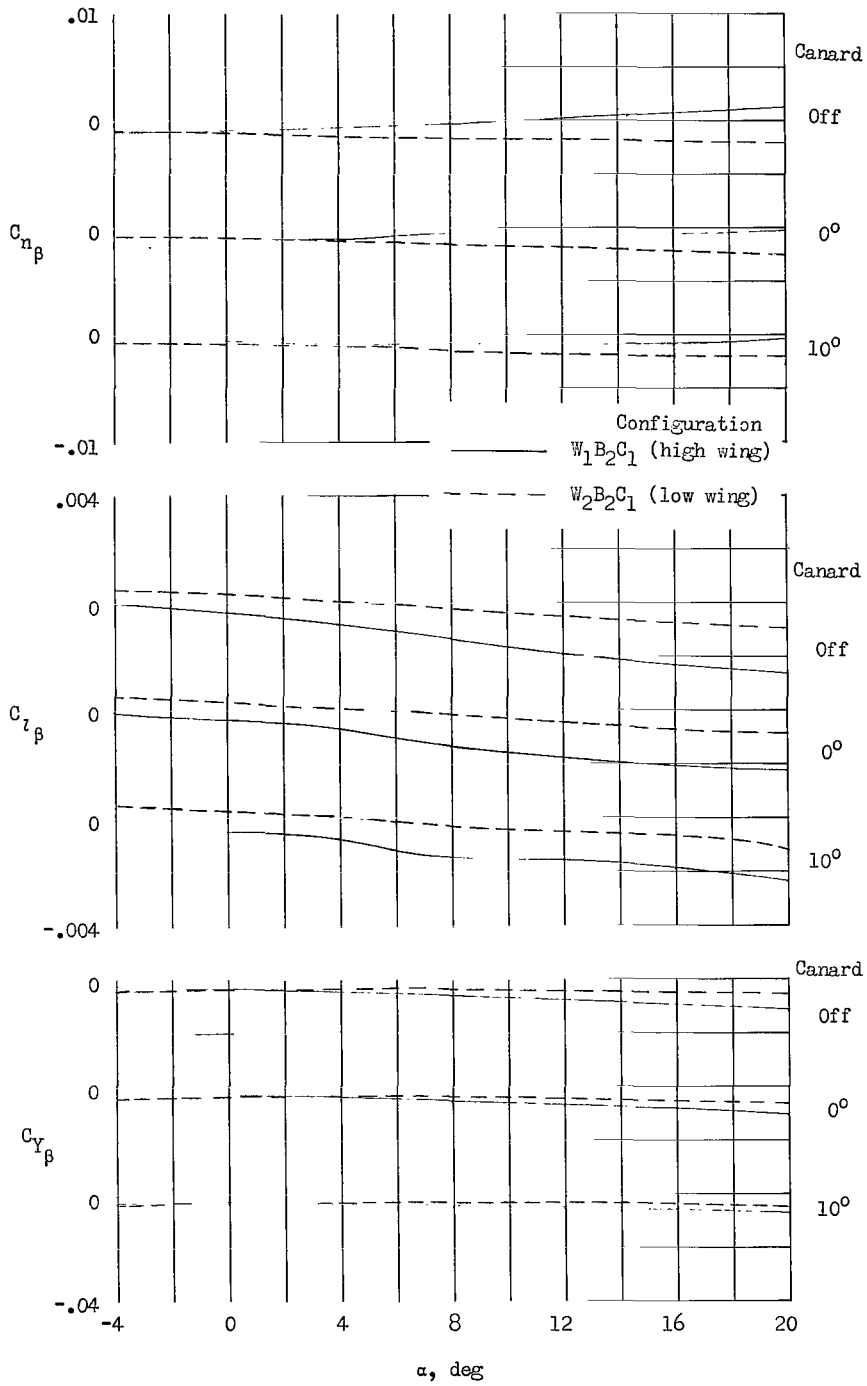

(a) Variation of stability derivatives with angle of attack. Vertical tails off.

Figure 28.- Effect of wing position on the directional and lateral aerodynamic characteristics of the long-nose small-delta-canard configuration.

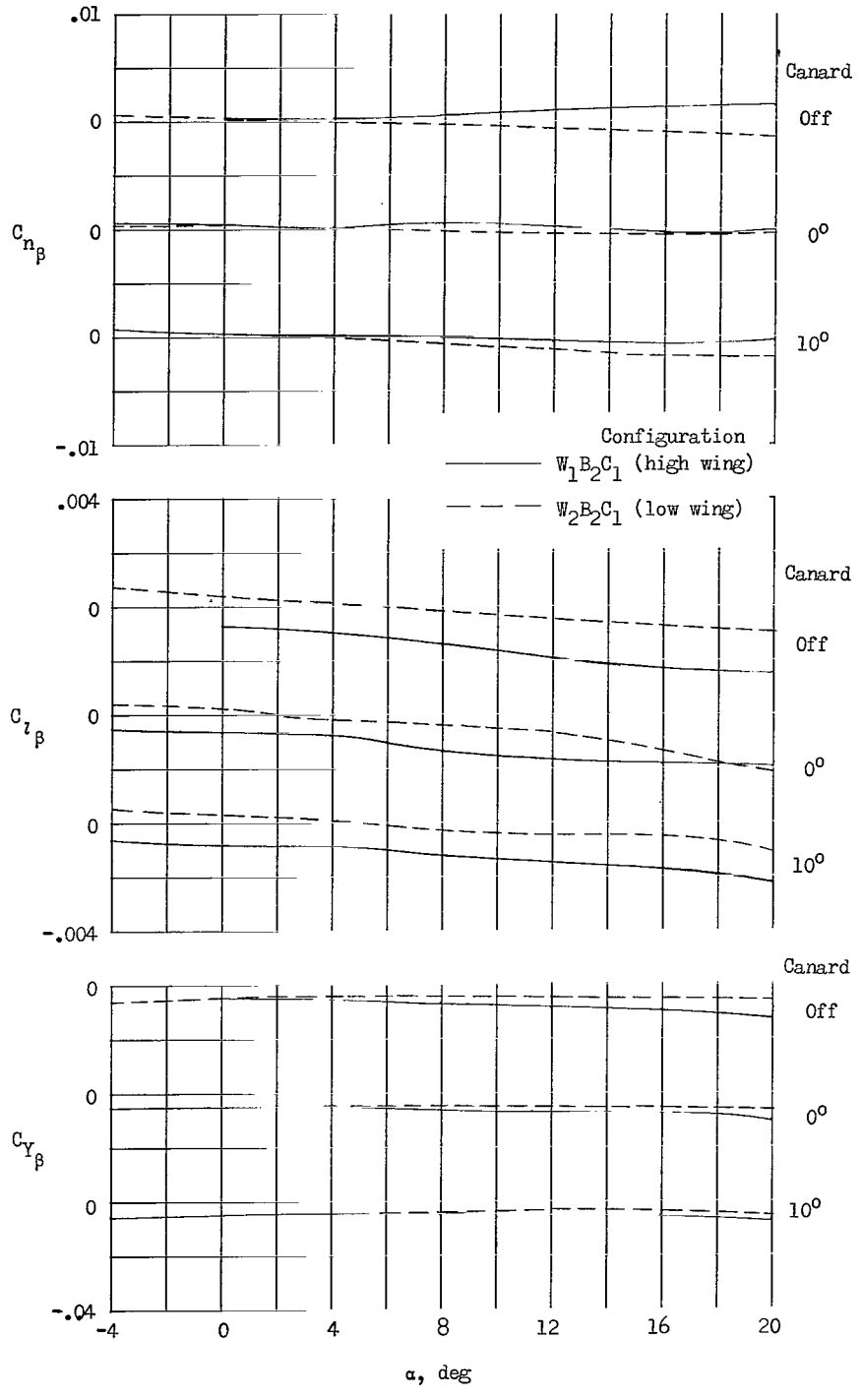

(b) Variation of stability derivatives with angle of attack. Vertical tails on.

Figure 28.- Concluded.

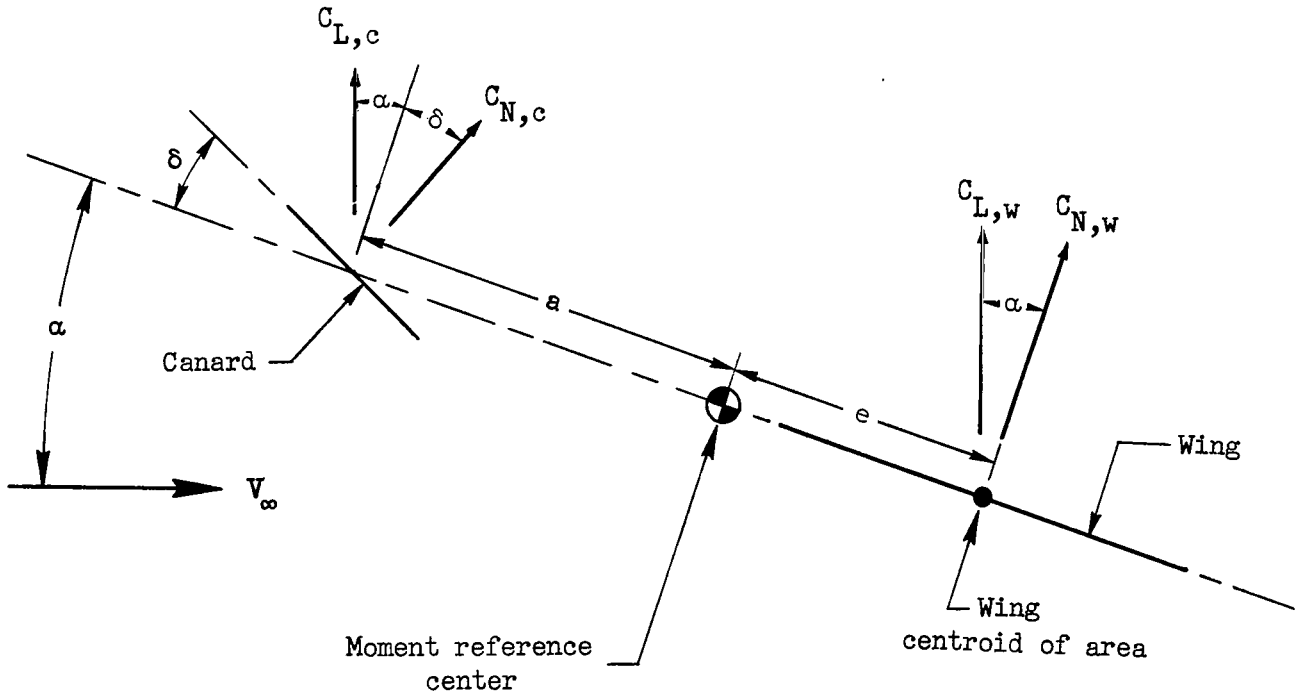

Figure 29.- Sketch showing the skeleton configuration used for Newtonian impact theory predictions of C_L and C_m on a canard configuration.

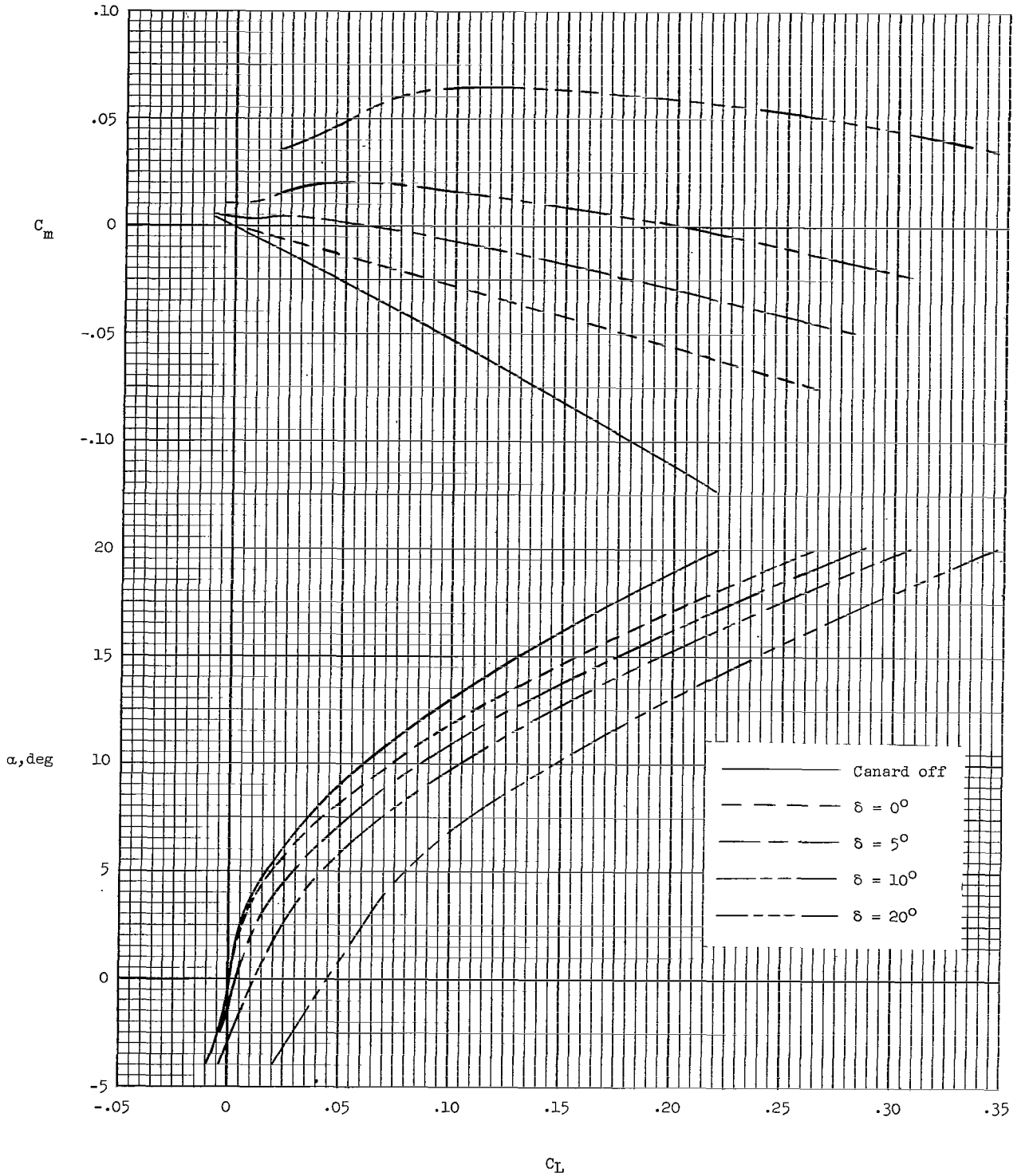

Figure 30.- Curves from Newtonian impact theory for the skeleton configuration of figure 29. $S_c/S = 0.20$; B_2; large canard.

"The aeronautical and space activities of the United States shall be conducted so as to contribute . . . to the expansion of human knowledge of phenomena in the atmosphere and space. The Administration shall provide for the widest practicable and appropriate dissemination of information concerning its activities and the results thereof."

—NATIONAL AERONAUTICS AND SPACE ACT OF 1958

NASA SCIENTIFIC AND TECHNICAL PUBLICATIONS

TECHNICAL REPORTS: Scientific and technical information considered important, complete, and a lasting contribution to existing knowledge.

TECHNICAL NOTES: Information less broad in scope but nevertheless of importance as a contribution to existing knowledge.

TECHNICAL MEMORANDUMS: Information receiving limited distribution because of preliminary data, security classification, or other reasons.

CONTRACTOR REPORTS: Technical information generated in connection with a NASA contract or grant and released under NASA auspices.

TECHNICAL TRANSLATIONS: Information published in a foreign language considered to merit NASA distribution in English.

TECHNICAL REPRINTS: Information derived from NASA activities and initially published in the form of journal articles.

SPECIAL PUBLICATIONS: Information derived from or of value to NASA activities but not necessarily reporting the results of individual NASA-programmed scientific efforts. Publications include conference proceedings, monographs, data compilations, handbooks, sourcebooks, and special bibliographies.

Details on the availability of these publications may be obtained from:

SCIENTIFIC AND TECHNICAL INFORMATION DIVISION

NATIONAL AERONAUTICS AND SPACE ADMINISTRATION

Washington, D.C. 20546